SMRT analysis of MTOC and nuclear positioning reveals the role of EB1 and LIC1 in single-cell polarization

Christopher M. Hale[1,2], Wei-Chiang Chen[1,2], Shyam B. Khatau[1,2], Brian R. Daniels[1], Jerry S. H. Lee[1,3] and Denis Wirtz[1,2,*]

[1]Department of Chemical and Biomolecular Engineering, The Johns Hopkins University, 3400 N. Charles St., Baltimore, MD 21218, USA
[2]Johns Hopkins Physical Sciences - Oncology Center, The Johns Hopkins University, 3400 N. Charles St., Baltimore, MD 21218, USA
[3]Center for Strategic Scientific Initiatives, Office of the Director, National Cancer Institute, National Institute of Health, Bethesda, MD 20892, USA
*Author for correspondence (wirtz@jhu.edu)

Accepted 12 August 2011
Journal of Cell Science 124, 4267–4285

doi: 10.1242/jcs.091231

Summary

In several migratory cells, the microtubule-organizing center (MTOC) is repositioned between the leading edge and nucleus, creating a polarized morphology. Although our understanding of polarization has progressed as a result of various scratch-wound and cell migration studies, variations in culture conditions required for such assays have prevented a unified understanding of the intricacies of MTOC and nucleus positioning that result in cell polarization. Here, we employ a new SMRT (for sparse, monolayer, round, triangular) analysis that uses a universal coordinate system based on cell centroid to examine the pathways regulating MTOC and nuclear positions in cells plated in a variety of conditions. We find that MTOC and nucleus positioning are crucially and independently affected by cell shape and confluence; MTOC off-centering correlates with the polarization of single cells; acto-myosin contractility and microtubule dynamics are required for single-cell polarization; and end binding protein 1 and light intermediate chain 1, but not Par3 and light intermediate chain 2, are required for single-cell polarization and directional cell motility. Using various cellular geometries and conditions, we implement a systematic and reproducible approach to identify regulators of MTOC and nucleus positioning that depend on extracellular guidance cues.

Key words: MTOC positioning, Nucleus positioning, Cell migration, Cell polarization, Cell biophysics, Cell shape

Introduction

Cell migration is required for a variety of physiological processes ranging from embryonic and adult development to healthy immune function (Trinkaus, 1984). Individual cells must polarize or organize their internal organelles to efficiently move from one position to another during migration. Cell polarization is thus essential for cell migration (Nobes and Hall, 1999), neuronal proliferation, migration and differentiation (Higginbotham and Gleeson, 2007), and is also tightly regulated during the epithelial–mesenchymal transition (EMT) in formation of the body plan and tissue development. Loss of this regulation can deleteriously manifest as disease, leading to organ fibrosis or cancer progression (Thiery et al., 2009). Although several proteins have been identified as regulators of the cell polarization pathway, their roles have yet to be explored in a variety of cellular microenvironments – a fundamental physiological variable that can directly affect cell shape and polarity (Thery, 2010) as well as the cell division plane (Minc et al., 2011).

Cellular polarization is largely determined by the location of the centrosome, or microtubule-organizing center (MTOC), relative to the nucleus. Epithelial cells maintain basal–apical polarity by positioning their centrosome above the nucleus (Bacallao et al., 1989), whereas in several other cell types, including astrocytes, fibroblasts and epithelial sheets, the centrosome is relocated between the nucleus and the leading edge of the cell during migration (Etienne-Manneville and Hall, 2001; Gotlieb et al., 1981; Kupfer et al., 1982). The Golgi complex colocalizes with the MTOC (Kupfer et al., 1982) and the positioning of these two organelles towards the leading edge of the cell probably contributes to the targeted delivery of processed proteins along microtubules towards the cell front (Bergmann et al., 1983).

Cell polarization can be stimulated by biochemical (Nemere et al., 1985) and electrical stimuli (Zhao et al., 2006), shear stress (Hale et al., 2008; Lee et al., 2005; Tzima et al., 2003) and environments that encourage cell migration, such as scratch-wound assays (Todaro et al., 1965). In the scratch-wound assay, which is widely used to study cell polarization, cells are grown to a confluent monolayer, scratched to create a zone devoid of cells, and cells at the wound edge are examined as they polarize and migrate to close the wound (Etienne-Manneville and Hall, 2001). Variations include the use of lysophosphatidic acid (LPA) or serum to stimulate either cell polarization or migration, respectively, of non-motile, serum-starved cells (Gomes et al., 2005). However, this assay requires that cells remain in close contact with one another, and thus does not permit the study of single-cell polarization. Although key mediators of MTOC and

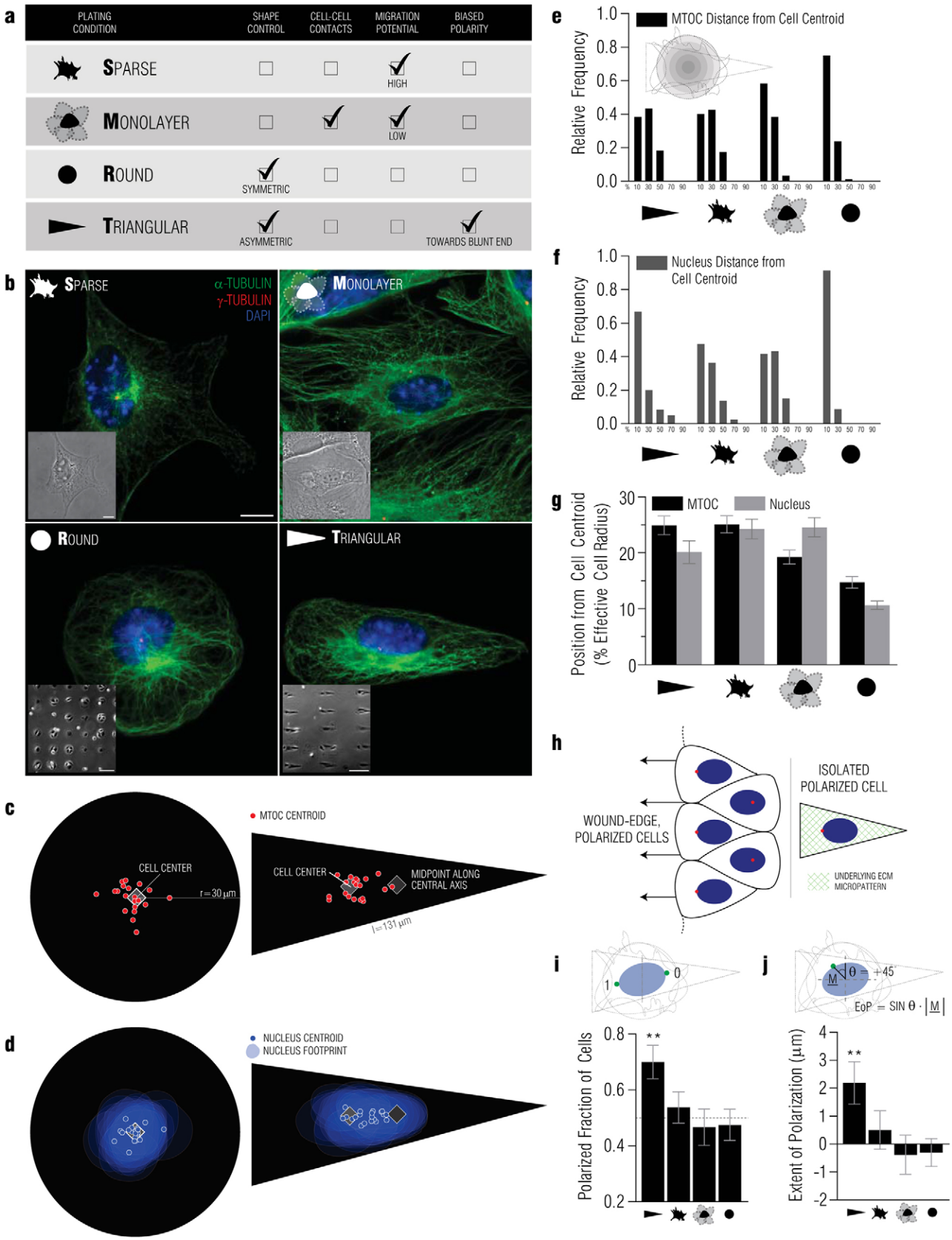

Fig. 1. See next page for legend.

nucleus positioning and cell polarization, namely integrins and the Cdc42–Par6–PKCζ complex (Etienne-Manneville and Hall, 2001), have been identified in in vitro scratch-wound assays with fibroblasts and astrocytes, little work has been done to investigate the role of these proteins and their downstream effectors in the context of single-cell polarization, which is more physiologically and pathologically relevant for these cell types. Furthermore, single-cell polarization events are prevalent in vivo during cell division (Lin et al., 2000), in colon carcinoma progression when single migratory cells lose E-cadherin expression (Thiery et al., 2009), in breast cancer metastasis (Giampieri et al., 2009), in fibrosarcoma cell invasion of the stroma (Wolf et al., 2003), and in the initial fibroblastic response to a wound to initiate the healing process and produce extracellular matrix proteins (Singer and Clark, 1999), among other in vivo physiological processes. Thus, it is important that we study the polarization of single cells in an environment free of cell–cell contact.

Together with the Cdc42–Par6–PKCζ complex and its downstream effectors, the filamentous proteins of the cytoskeleton, specifically actin and microtubules play a significant role in determining the position of the MTOC and nucleus in the cell (Bornens, 2008). Elegant experimental and computational studies have identified three primary forces that act on microtubules to position the MTOC in the cell – a strong dynein pulling force, a weak myosin-powered actin drag and an anti-centering force from microtubule growth in the cell (Burakov et al., 2003; Zhu et al., 2010). Nuclear positioning is also determined by microtubule and actin networks (Reinsch and Gonczy, 1998), to which the nucleus can directly tether through the linker of nucleoskeleton and cytoskeleton (LINC), complex proteins such as Sun and nesprin (Razafsky and Hodzic, 2009). Scratch-wound studies suggest that during polarizing events, the MTOC remains centered while the nucleus moves to a rear position, generating the polarized morphology in which the MTOC is positioned between the nucleus and the leading edge of the cell (Gomes et al., 2005). In this study, we confined cells to ECM micropatterns (Khatau et al., 2009; Thery and Piel, 2009), akin to cellular restriction in tissue, allowing us to assess to what extent the MTOC is truly centered in a regulated cellular geometry and to determine the extrinsic factors and internal proteins that affect MTOC and nucleus positioning as well as cell polarization in single cells. Cells were treated with cytoskeletal-interfering drugs or depleted of specific polarity proteins to assess the primary forces that regulate the positioning of these organelles. Previous studies have also demonstrated the necessity of cell–cell cadherin interactions in regulating cell polarization in contacting cells (Dupin et al., 2009), suggesting that single-cell polarization is probably achieved by a cadherin-independent mechanism that relies instead on integrin interaction with the extracellular matrix (Etienne-Manneville and Hall, 2001; Thery et al., 2006). Thus, we hypothesized that the mechanisms that the cell employs to position the MTOC and nucleus would vary with cellular shape and the presence of cell–cell contacts. To this end, we also plated cells in unpatterned sparse and confluent conditions and compared the results with those of single cells confined to defined geometries. By eliminating the confounding effects of cell–cell contacts in micropatterned conditions, we employed a systematic, highly reproducible approach to determine the proteins involved in single-cell polarization and identify regulators of MTOC and nucleus positioning that depend on extracellular guidance cues.

Fig. 1. Positions of MTOC and nucleus depend on cellular shape and confluence. (**a**) SMRT (sparse, monolayer, round and triangular) conditions in which cells were plated to vary factors thought to affect MTOC and nucleus positioning. (**b**) Immunofluorescence of microtubules (green), microtubule-organizing center (MTOC, red) and the nucleus (blue) in SMRT conditions. Scale bar: 10 μm. Insets: Phase contrast images of sparse (top left) and confluent cells (top right) at high-magnification. Scale bars: 10 μm. Low-magnification phase-contrast images show confinement of cells to circular (bottom left) and triangular (bottom right) micropatterns. Scale bars: 100 μm. (**c**,**d**) Actual MTOC (c) and nucleus (d) centroids in 20 randomly chosen cells overlaid on circular (left) and triangular (right) masks upon which cells were confined. (**e**) Frequency distribution of the distance of the MTOC from the cell centroid in triangular, sparse, confluent and circular cells. Cellular area was divided into five regions of equal radius such that the first bin centered at 10% represents the number of cells whose MTOCs were located within 20% of an effective radius of the cell (~6 μm for a circular cell) from the cell centroid ($n \geq 60$ cells for each condition). (**f**) Frequency distribution of the distance of the nucleus from the cell centroid in triangular, sparse, confluent and circular cells ($n \geq 60$ cells for each condition). (**g**) Average distances of the MTOC (black) and nucleus (gray) from the cell centroid in triangular, sparse, confluent and circular cells ($n \geq 60$ cells for each condition). (**h**) Diagrams of two in vitro polarization assays, the scratch-wound assay (left) and the single-cell micropatterning polarization assay (right). Note that wound-edge cells and the single cell are polarized as indicated by the forward position of the MTOC (red) relative to the nucleus (blue). (**i**) Fractions of cells that were polarized in polarized triangular, sparse, confluent, and circular cells assessed in a binary fashion such that MTOCs located to the left of the nucleus were scored as polarized and received a score of 1, whereas MTOCs located to the right of the nucleus were scored as unpolarized and received a score of 0, according to the ability of the triangular-shaped micropattern to polarize cells towards their blunt end (Jiang et al., 2005) ($n \geq 60$ cells for each condition). (**j**) Extents of polarization of triangular, sparse, confluent and circular cells. Asterisks in i and j indicate that a population is significantly ($P < 0.01$) polarized, compared to unpolarized population-based theoretical means of 0.5 and 0.0, respectively, using a one-sample *t*-test ($n \geq 60$ cells for each condition).

Results

MTOC and nucleus position independently depend on cellular shape and confluence

Using mouse embryonic fibroblasts (MEFs) as a model, we investigated the subcellular position of the MTOC and the nucleus to establish the molecular and physical mechanisms of cell polarization and determined the robustness of MTOC centering. Fibroblasts were plated in either sparse or confluent conditions on fibronectin-coated substrates and on cell-sized circular and triangular fibronectin micropatterns to investigate the effects of both cell–cell contacts and cellular shape on determining the positions of the MTOC and nucleus (Fig. 1a,b). The use of circular and triangular micropatterns allowed us to tightly regulate cell shape and avoid confounding effects of shape heterogeneity often present in sparsely plated cells (see supplementary material Fig. S1). Cells were allowed to adhere for 3 hours, after which they were fixed; positions of nuclei and MTOC were subsequently determined using immunofluorescence microscopy by staining nuclear DNA with DAPI and γ-tubulin and an anti-γ-tubulin antibody.

Surprisingly, a large number of MTOCs were positioned more than 20% of the effective radius of the cell away from the cell center (>6 μm from the center of cells placed on circular patterns), which occurred in all plating conditions (Fig. 1e). Only in confluent and circular cells were a majority of MTOCs found

within the most central region of the cell, defined as a circle 12 μm in diameter (20% of the effective diameter of the cell). The average distance between MTOC and cell centroid was lowest in circularly micropatterned cells (Fig. 1g), but even here, MTOCs were routinely found microns away from the cell center. The MTOCs in circular cells crowded at the cell center, whereas MTOCs in triangular cells were more likely to be located between the cell center and the midpoint along the central axis of the triangle (see randomly chosen MTOC positions in 20 circular and triangular cells in Fig. 1c). Accordingly, the average distance between the MTOC and the cell centroid was significantly higher in triangular cells than in circular cells ($P<0.001$). These results indicate that the MTOC is typically not positioned at the geometric center of cells and that the distance between MTOC and cell centroid depends both on the overall shape of the cell and the presence of cell–cell contacts.

In contrast to MTOCs, nucleus centroids were positioned closer to the cell center in all considered conditions, except in confluent cells (Fig. 1g), with nuclei being most centered in circular cells (11±1% of effective cell radius from center) and least centered in both sparse and confluent cells (24±2% and 25±2% of effective cell radius from center, respectively). Interestingly, the positions of MTOC and nucleus did not correlate with one another. These results suggest that, whereas MTOC and nucleus positions depend on cell shape and confluence, their positions are regulated by distinct pathways, even though the two organelles are likely to be physically coupled through LINC complex proteins and emerin (Crisp et al., 2006; Hale et al., 2008; Salpingidou et al., 2007). This linkage is also likely to be dynamic, allowing the MTOC and nucleus to move in opposing directions while maintaining a physical connection.

Polarizing single cells with asymmetric ECM micropatterns

The use of micropatterns allowed us to systematically assess the ability of cells to polarize, as judged by the position of the MTOC relative to that of the nucleus centroid in single cells. In several cell types, including fibroblasts and astrocytes, the MTOC is positioned between the nucleus and the leading edge of the cell during migration (Etienne-Manneville and Hall, 2001; Euteneuer and Schliwa, 1992; Gundersen and Bulinski, 1988; Kupfer et al., 1982; Palazzo et al., 2001). Although the wound-healing assay provides a convenient environment to study cell polarization, it requires cells to be in contact with one another (see Fig. 1h, left), and thus, possible contributions from cell–cell contacts cannot be decoupled from the polarization process. Alternatively, micropatterning with asymmetric geometries similar in shape to wound-edge cells (see Fig. 1h, right) functionally polarizes single cells such that they will migrate in the direction in which they are polarized once released from the micropatterns to which they are originally confined (Jiang et al., 2005). Indeed, 70% of cells plated on triangular fibronectin micropatterns were polarized towards the blunt end of the shape as determined by binary scoring (Fig. 1i), representing a statistically significant difference compared with a theoretically unpolarized population of cells ($P<0.01$, one sample *t*-test compared to a theoretical mean of 0.5). Conversely and as expected, cells on circles – a symmetric geometry – did not favor polarization towards the left or right (48±6% polarized to the left) and were not significantly polarized ($P=0.51$, one sample *t*-test compared to a theoretical mean of 0.5). Additionally, although sparse and confluent cells are probably individually polarized along cell-specific axes, neither sparse nor confluent cell populations were deemed polarized, as assessed by the vertical polarity axis that was applied across all SMRT conditions. Note that although this vertical axis is relevant in the case of triangular cells, it functions as an arbitrary axis for sparse, confluent and round cells.

Polarization was also assessed more quantitatively using a metric that reflects the extent to which the MTOC is displaced from the nucleus center. This metric was termed ‘extent of polarization’ (Fig. 1j), and is positive when the MTOC is displaced to the left and negative when the MTOC is displaced to the right. In triangular cells, the extent of polarization was 2.2±0.8 μm, reflecting a morphologically polarized cell. Again, the population mean was significantly different from a theoretically unpolarized population of cells ($P<0.01$, one sample *t*-test compared to a theoretical mean of 0.0), whereas the extent of polarization in circular cells was negligible (−0.3±0.5 compared to a m) indicating that the cells were unpolarized. As expected, the difference between the mean extent of polarization in circular cells and that of a theoretically unpolarized population of cells was not statistically significant ($P>0.05$). The extent of polarization of cell populations agreed well with the fraction of the cells that were polarized (Fig. 1i,j) and provided a quantitative means to distinguish the degree to which two cells differed in polarization, even if both received the same binary polarization score.

Interestingly, MTOC position was highly correlated with cell polarization: distances between MTOC and cell centroid were larger in cells plated on polarizing shapes (e.g. isosceles triangles) and smaller in cells plated on symmetrical, non-polarizing shapes (e.g. circles; Fig. 1g,i,j). Thus, in polarized cells, the MTOC was positioned between the leading edge and the nucleus, as is the case in several migrating cell types (Etienne-Manneville and Hall, 2001; Li and Gundersen, 2008; Manneville and Etienne-Manneville, 2006; Palazzo et al., 2001; Tsai et al., 2007). However, the MTOC was not maintained in a central position in this geometry. In triangular cells, the mean MTOC position was 25±2% of the effective cell radius from the cell centroid. Together these results suggest that the cellular polarization machinery functions in distinct modes depending on whether the cell is isolated or in contact with other neighboring cells.

Cellular forces affecting MTOC and nucleus positioning

Several forces within the cell act to regulate the positioning of the MTOC and the nucleus. Although some of these forces, namely those acting on microtubules to affect MTOC positioning, have been previously suggested (Zhu et al., 2010), their direct roles have yet to be fully explored in the context of differing cellular microenvironments. These forces include, but are not limited to: (1) the outward growth of microtubules, which upon impacting the cell membrane, generate an inward pushing force on the MTOC from which they emanate; (2) the stabilizing force maintained by Sun and ZYG-12-homologous nesprin proteins of the LINC complex to connect the nucleus to the cytoskeleton and possibly the MTOC directly to the nucleus (Malone et al., 2003); (3) dynein motors, localized to either the plasma membrane or cytoskeletal structures, that pull on microtubules, resulting in an outward pulling force on the MTOC; (4) retrograde actin flow caused by actin microfilament polymerization at the cell periphery that exerts an inward pushing force on both the MTOC

and nucleus; (5) adhesion molecules (e.g. cadherins) at cell–cell contacts that recruit multiprotein complexes and cytoskeletal contacts to form mature bonds between cells (Bajpai et al., 2008); and (6) the effect of cell shape that alters the above forces according to cellular geometry. To investigate the roles of these forces and assess their impact in various cellular geometries in both single and confluent cells, experiments were carried in which cytoskeletal structures were depolymerized or specific proteins were inhibited or depleted.

Actin and myosin II regulate MTOC and nuclear position in a cell shape- and cell–cell-contact-dependent manner

Although microtubule growth and dynamics can directly affect MTOC positioning, the actin cytoskeleton can also affect MTOC positioning through cytoskeletal linkers such as plectin (Svitkina et al., 1996) that couple microtubules to myosin-powered actin retrograde flow (Zhu et al., 2010). Actin retrograde flow can also directly affect nuclear positioning through Sun and nesprin proteins of the LINC complex, which directly connects the nuclear envelope to the cytoskeleton (Razafsky and Hodzic, 2009). Thus, we investigated the role of actin and the force-generating motor protein myosin II in the regulation of MTOC and nucleus positioning with specific inhibitory drugs. Actin was depolymerized using latrunculin B (0.5 μM), myosin II was specifically inhibited with blebbistatin (25 μM), and myosin light chain kinase (MLCK), an activator of myosin II activity, was inhibited with ML-7 treatment (20 μM). Blebbistatin can also block actin retrograde flow (Ponti et al., 2004; Waterman-Storer and Salmon, 1997), which has been implicated in regulating nuclear positioning (Gomes et al., 2005) as well as MTOC positioning through microtubule–actin interactions (Zhu et al., 2010). Actin staining (Fig. 2a) was performed in latrunculin B-, blebbistatin- and ML-7-treated cells to verify drug effects on actin bundling and microfilament structure; staining agreed well with staining patterns seen in similarly treated 3T3 fibroblasts (Hale et al., 2009). When treated with these drugs, MTOC position was least affected in circular and triangular cells, whereas MTOCs in sparse cells were located significantly closer to the cell centroid and MTOCs in confluent cells were consistently positioned farther from the cell centroid than in untreated cells (Fig. 2b, black bars; 2c). These results suggest that actin, MLCK, and myosin II not only play roles in MTOC positioning, but also that the specific roles of these proteins are dependent on whether a cell is isolated or in contact with neighboring cells.

Latrunculin B, blebbistatin and ML-7 treatments had little effect on nuclear position in confluent cells (Fig. 2d). In sparse and triangular cells, however, nuclei were consistently found closer to the cell centroid, whereas nuclei in circular cells were located farther from the cell centroid (Fig. 2b, gray bars; 2d). These results correlate with the polarizing potential of each shape. The distance of the nucleus from the cell centroid was less in polarizing conditions, or when cells adhered to triangular micropatterns, whereas the nucleus was positioned farther from the cell center in unpolarizing conditions, or when cells adhered to circular micropatterns. These results suggest that actin and myosin II play roles in off-centering the nucleus in polarized cells and maintaining the nucleus in a directionally unbiased position, i.e. the center, in unpolarized cells.

Although the effects of myosin-inhibiting drugs blebbistatin (directly) and ML-7 (indirectly through inhibition of myosin light chain kinase) were similar in nearly all cases, it is important to note that the effect of latrunculin B treatment on MTOC and nucleus position closely matched that of blebbistatin and ML-7 across plating conditions, e.g. the changes in nucleus position in circular cells were similar in magnitude for latrunculin B-, blebbistatin- and ML-7-treated cells. Furthermore, the fraction of the triangular cells that were polarized was reduced to nearly half by all drug treatments (Fig. 2e). Similarly, latrunculin B, blebbistatin and ML-7 treatment reduced the polarization of triangular cells to negligible levels (Fig. 2f). Though the effects of these drugs on MTOC and nucleus positioning differed across sparse, confluent, circular and triangular cells, our results suggest that actin and myosin function in unison to regulate cell polarization through MTOC and nucleus positioning, because depolymerization or inhibition of either actin or myosin alone contributes to positional changes and loss of polarization.

Microtubules and microtubule dynamics are required for MTOC positioning in a cell shape- and cell–cell contact-dependent manner

Next, we examined the role of microtubules in MTOC and nucleus positioning. Because the MTOC is the nucleation site for microtubule assembly (Doxsey, 2001) and thus both the MTOC and microtubules are tightly connected, we hypothesized that MTOC position would be significantly affected by microtubule disassembly. Previous studies in epithelial cells suggested that the MTOC is centrally positioned by a balance of dynein pulling forces generated at the cell cortex that act on microtubules (Burakov et al., 2003). Computational studies further suggested that the position of the MTOC is determined largely by dynein pulling forces acting along the length of microtubules together with retrograde actin flow coupled to the microtubule network and the force of microtubules growing and pushing against the plasma membrane (Zhu et al., 2010). Eliminating these pushing and pulling forces through nocodazole treatment should then disrupt this balance and unless all microtubules are depolymerized simultaneously, this treatment is likely to increase the MTOC position from the cell centroid. To investigate the role of microtubules in the positioning of the MTOC and nucleus, cells were treated with 3.3 μM nocodazole, which depolymerizes microtubules (Fig. 3a, upper panels). For all considered cell shape and confinement conditions, nocodazole treatment increased the distance between the MTOC and cell centroid compared with untreated cells (Fig. 3b, black bars). The distance between MTOC and cell centroid increased most in circular cells (+80±9%), was moderately increased in confluent and triangular cells (+40±10% and +47±9%, respectively), but increased only slightly in sparse cells (+6±6%; Fig. 3c, upper panel). The effect of nocodazole treatment on nuclear position was much more varied, with nuclei in sparse cells becoming more centered, nuclei in circular cells less centered and nuclei in confluent and triangular cells showing negligible changes in position (Fig. 3b, gray bars; 3d, upper panel). These results suggest that the role of microtubules and the forces acting on them in regulating MTOC and nuclear positioning are highly dependent on extracellular guidance cues, including the presence of other cells and cellular shape.

Next, the role of microtubule dynamics was studied by stabilizing microtubules with Taxol (1 μM; Fig. 3a, lower panels), which blocks the dynamic instability of microtubules by stabilizing GDP-bound tubulin (Schiff et al., 1979). Taxol

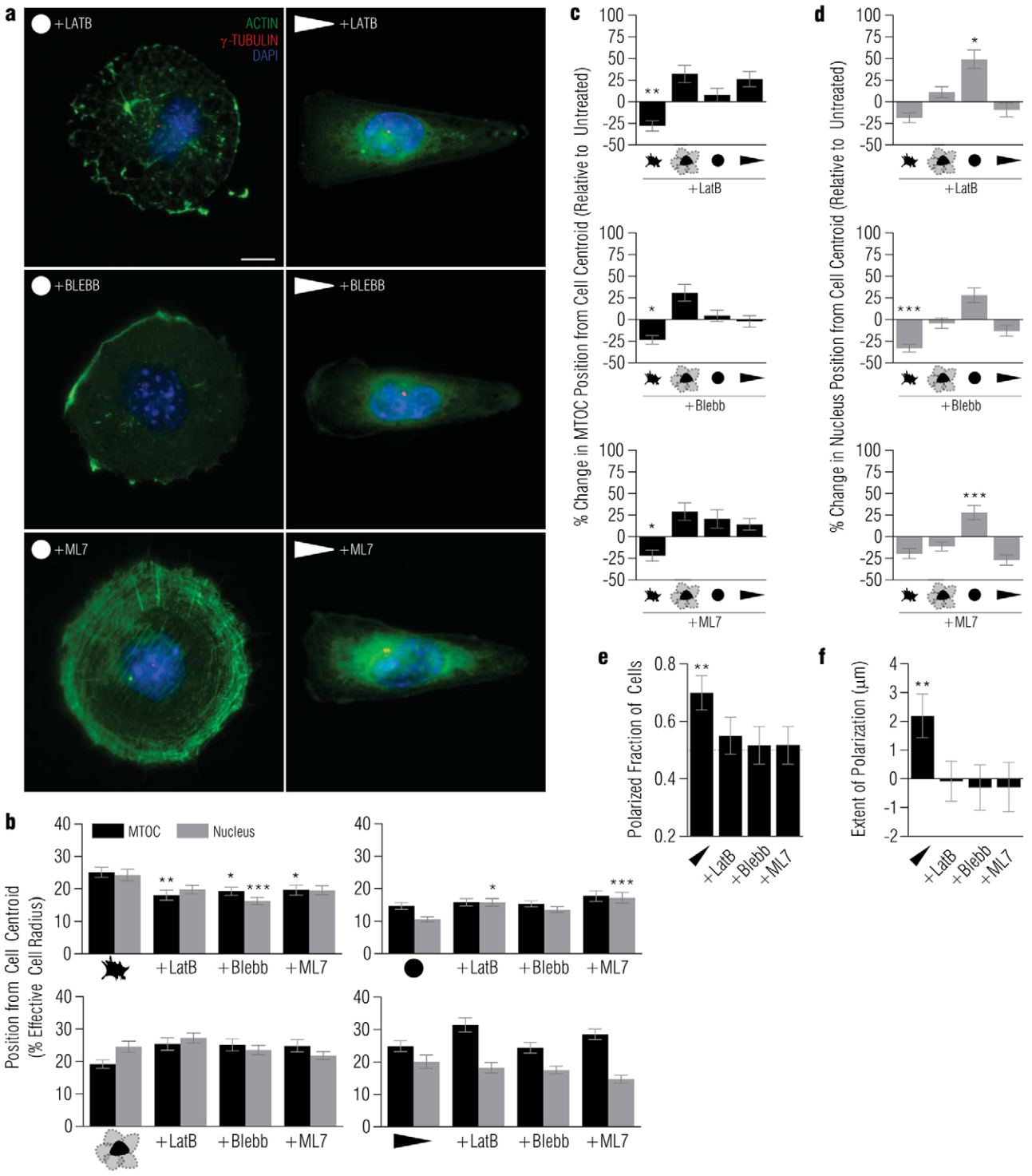

Fig. 2. Actin- and myosin-mediated MTOC and nucleus positioning depend on cell shape and confluence. (**a**) Immunofluorescence of actin (green), MTOC (red) and the nucleus (blue) in latrunculin B-treated circular (top left) and triangular cells (top right), blebbistatin-treated circular (middle left) and triangular cells (middle right) and ML-7-treated circular (bottom left) and triangular cells (bottom right). Scale bar: 10 μm. (**b**) Average MTOC (black) and nucleus (gray) distances from the cell centroid in untreated, latrunculin-B-treated, blebbistatin-treated and ML-7-treated SMRT conditions ($n \geq 60$ cells for each condition). (**c**,**d**) Percentage change in the distance of the in MTOC (c) and nucleus (d) from the cell centroid upon latrunculin B (top), blebbistatin (middle) and ML-7 treatment (bottom), relative to untreated cells in SMRT conditions ($n \geq 60$ cells for each condition). (**e**) Fractions of cells that were polarized in untreated, latrunculin-B-, blebbistatin- and ML-7-treated cells plated on triangular micropatterns ($n \geq 60$ cells for each condition). (**f**) Extents of polarization of untreated, latrunculin-B-, blebbistatin- and ML-7-treated cells plated on triangular micropatterns ($n \geq 60$ cells for each condition). *$P<0.05$; **$P<0.01$; ***$P<0.001$.

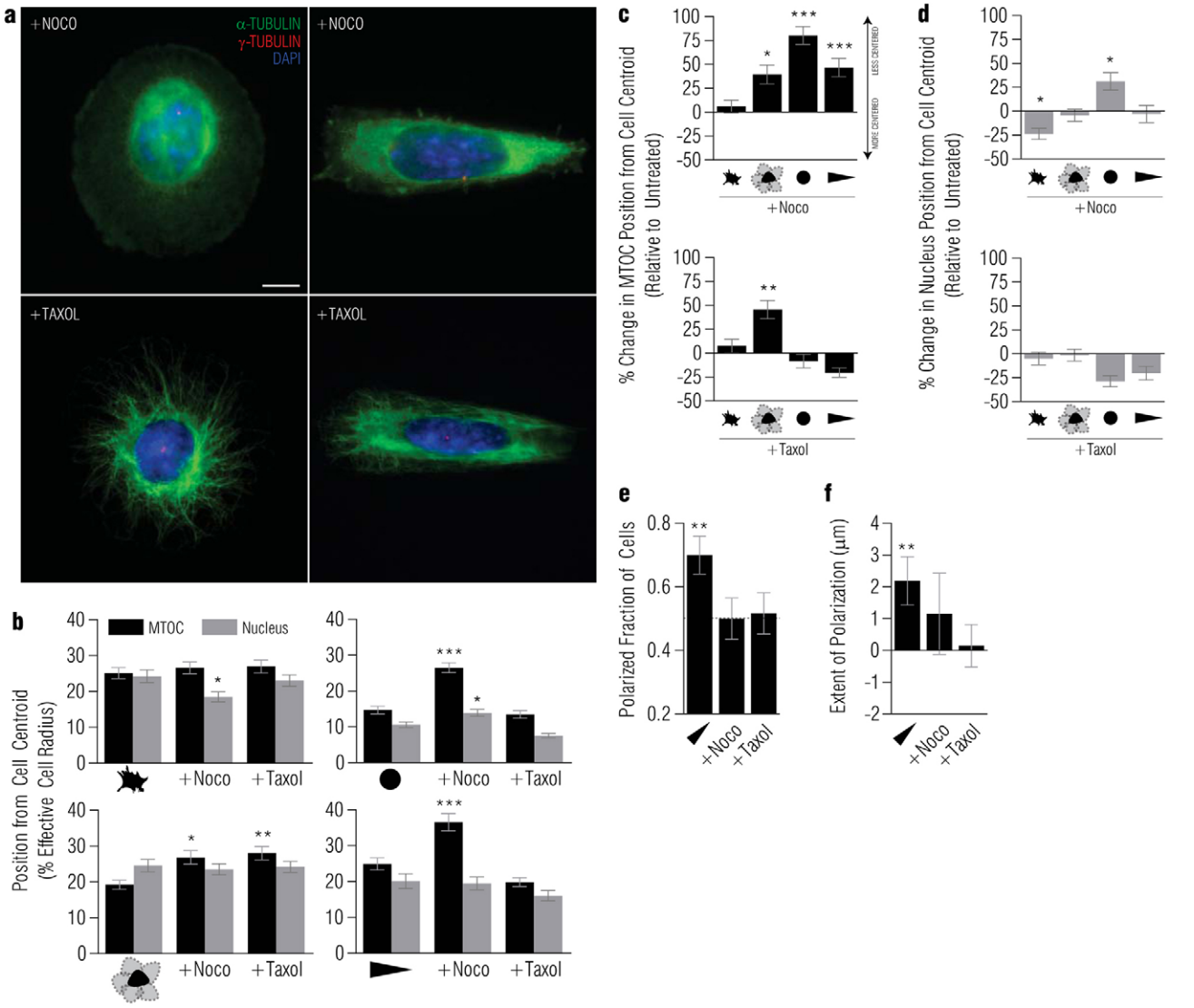

Fig. 3. Microtubule-mediated MTOC and nucleus positioning depends on cell shape and confluence. (**a**) Immunofluorescence of microtubules (green), MTOC (red) and the nucleus (blue) in nocodazole-treated circular (top left) and triangular cells (top right) and Taxol-treated circular (bottom left) and triangular cells (bottom right). Scale bar: 10 μm. (**b**) Average distance of the MTOC (black) and the nucleus (gray) from cell centroid in untreated, nocodazole-treated and Taxol-treated SMRT conditions. Asterisks indicate significant differences (*P<0.05; **P<0.01; ***P<0.001) between the indicated population and untreated cells using a one-way ANOVA followed by Dunnett's multiple comparison test (n≥60 cells for each condition). (**c**,**d**) Percentage change in the distance of the MTOC (c) and the nucleus (d) from the cell centroid upon nocodazole (top) and Taxol treatment (bottom) relative to untreated cells in SMRT conditions (n≥60 cells for each condition). (**e**) Fractions of cells that were polarized in untreated, nocodazole- and Taxol-treated cells plated on triangular micropatterns (n≥60 cells for each condition). (**f**) Extents of polarization of untreated, nocodazole- and Taxol-treated cells plated on triangular micropatterns (n≥60 cells for each condition).

treatment largely concentrated microtubules around the cell center and formed a dense microtubule ring around the nucleus in both circular and triangular cells, leaving the periphery devoid of microtubules (compare Fig. 3a, lower panels and 3b, lower panels). Although microtubule structure was qualitatively different upon Taxol treatment it had little effect on the position of the MTOC and nucleus in all tested conditions compared with nocodazole treatment (Fig. 3b; 3c, bottom panel; 3d, bottom panel), with the exception of confluent cells, in which MTOC–cell centroid distance significantly increased relative to untreated cells (Fig. 3b, bottom left panel; 3c, bottom panel; P<0.01). These results suggest that microtubule dynamics play a more significant role in positioning the MTOC in confluent cells than in single cells, and reinforces the notion that microtubule dynamics at cell–cell contacts play a central role in the molecular mechanisms regulating the position of the MTOC (Schmoranzer et al., 2009).

Both nocodazole and Taxol treatments reduced the fraction of polarized cells and reduced the average extent of polarization when cells adhered to triangular micropatterns (Fig. 3e,f). Whereas the inability of nocodazole-treated triangular cells to effectively polarize was expected because of the significant increase in distance of the MTOC from the cell centroid relative to the nucleus position in control cells, the effect of Taxol in preventing polarization was unexpected considering that neither MTOC– nor nucleus–cell centroid distance was significantly

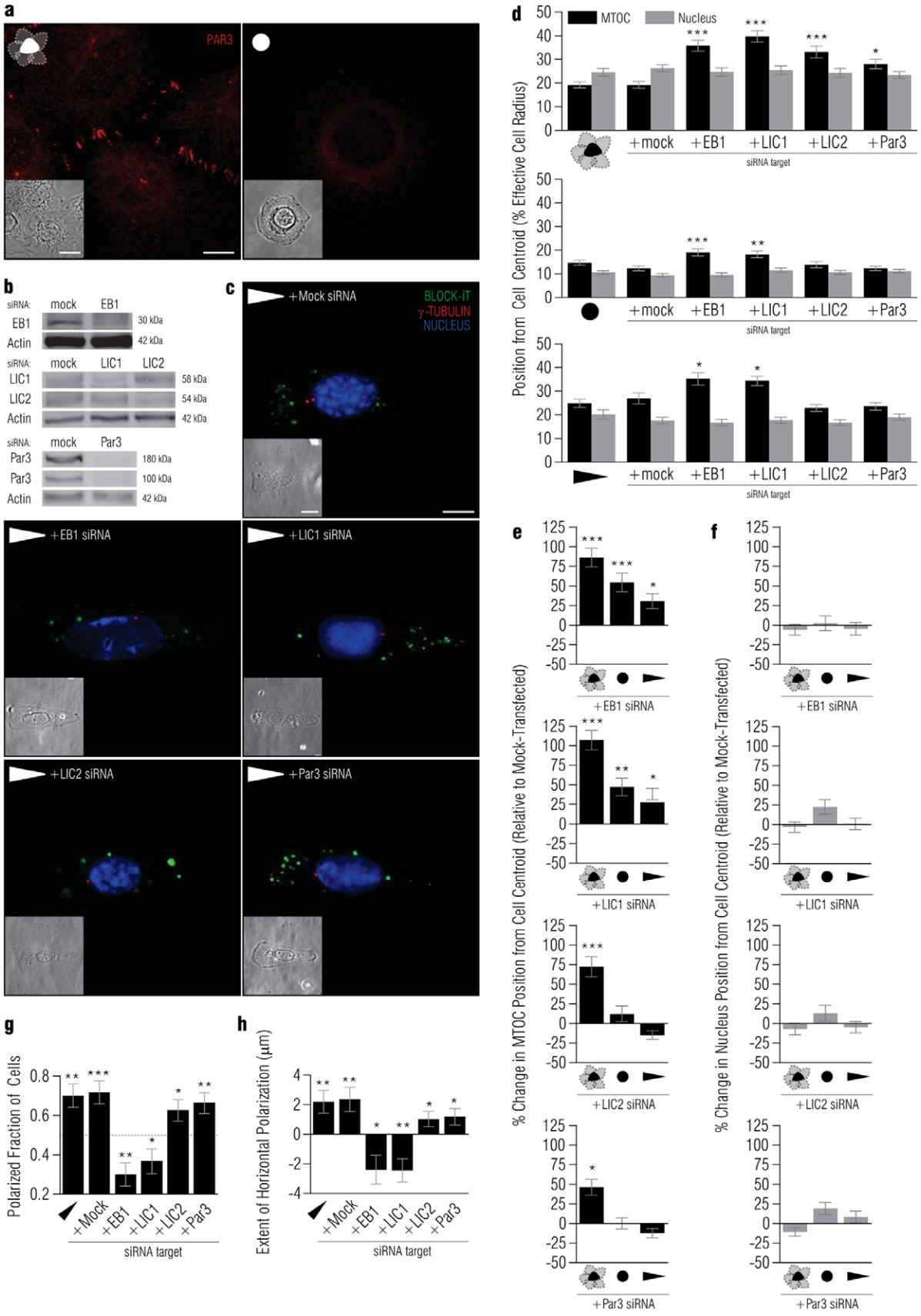

Fig. 4. See next page for legend.

different from untreated cells (Fig. 3b, bottom right panel; Fig. 3c, bottom panel). Taxol treatment did, however, marginally decrease the distance of both the MTOC and nucleus from the cell centroid in triangular cells, and thus these decreased distances were sufficient to reduce both cell polarization (Fig. 3e) and the extent of polarization (Fig. 3f).

LIC2 and Par3 regulate MTOC positioning and polarization only in confluent cells

We next targeted specific proteins that directly or indirectly interact with microtubules to coordinate cell polarity. Previous work has demonstrated the requirement of dynein light intermediate chain 2 (LIC2) and the partitioning-defective protein Par3 in polarization of confluent, wound-edge fibroblasts (Schmoranzer et al., 2009), but the roles of these proteins have yet to be explored in single-cell polarization. Because dynein and Par3 interact near cell–cell contacts (Schmoranzer et al., 2009), we hypothesized that these proteins would not play a role in the polarization of isolated triangular cells lacking such contacts. Indeed, Par3 formed zipper-like structures across cell–cell contacts in confluent fibroblasts (Fig. 4a, left panel), but no such structures were observed in single circular cells (Fig. 4a, right panel) or in isolated sparse or triangular cells (not shown). To quantitatively investigate the roles of these proteins in MTOC and nucleus positioning and cell polarization, we utilized short interfering RNA (siRNA) oligonucleotides to selectively reduce expression of LIC2 by ~50% and the 180 kDa and 100 kDa isoforms of Par3 by ~80% and ~60%, respectively (Fig. 4b). LIC2 knockdown was specific and did not affect LIC1 levels (Fig. 4b). The MTOC–cell centroid distance in confluent LIC2- and Par3-depleted cells was significantly increased relative to that in confluent mock-transfected cells (+70±10% and +46±10%, respectively; $P<0.001$ and $P<0.05$, respectively; Fig. 4d, top panel, black bars; 4e, lower panels), whereas the nucleus position was unaffected (Fig. 4d, top panel, gray bars; 4f, lower panels). The MTOC–cell centroid distance in both circular and triangular cells, however, was not significantly affected by LIC2 and Par3 depletion (+12±10% and 0±7% in circles, respectively; –18±6% and –11±7% in triangles, respectively; Fig. 4d, middle and bottom panels, black bars; 4e, lower panels). Moreover, nucleus position was largely unaffected in these cells (Fig. 4d, middle and lower panels, gray bars; 4f, lower panels). Furthermore, LIC2- and Par3-depleted fibroblasts were able to polarize on triangular micropatterns and had positive average extents of polarization (Fig. 4g,h). These results indicate that LIC2 and Par3, although required for polarization of confluent, wound-edge cells, are not essential for the polarization of single cells, which lack cell–cell contacts.

Fig. 4. EB1, LIC1 and 2 and Par3 regulate MTOC and nuclear positioning in a cell-confluence-dependent manner.
(**a**) Immunofluorescence of Par3 (red) in confluent cells (left) and an isolated, circular cell (right). Note the zipper-like structures that form at cell–cell contacts in confluent cells, and the absence of these structures at the cell periphery in the isolated circular cell. Scale bar: 10 μm. Insets: corresponding phase-contrast images of confluent cells (left) and an isolated, circular cell (right). Scale bar: 20 μm. (**b**) Immunoblots of EB1 and actin (loading control) from MEFs transfected with EB1 and mock siRNAs (top); immunoblots of LIC1, LIC2 and actin from MEFs transfected with LIC1, LIC2 and mock siRNAs (middle); immunoblots of Par3 and actin from MEFs transfected with Par3 and mock siRNAs (bottom). (**c**) Immunofluorescence of Block-iT Fluorescent Oligo (green), MTOC (red) and DRAQ5- or DAPI-stained nuclei (blue) in siRNA-transfected cells on triangular micropatterns. Scale bar: 10 μm. Insets: corresponding phase-contrast images (bottom left). Scale bar: 20 μm. (**d**) Average distance of the MTOC (black) and nucleus (gray) from the cell centroid in fibroblasts transfected with mock siRNA and siRNA targeted at EB1, LIC1, LIC2 and Par3. Results are shown for confluent (top), circular (middle) and triangular cells (bottom; $n\geq60$ cells for each condition). (**e**,**f**) Percent change in the distance of the MTOC (e) and nucleus (f) from the cell centroid in EB1- (top), LIC1- (top middle), LIC2- (bottom middle) and Par3-siRNA-treated cells (bottom) relative to mock-siRNA treated cells in confluent, circular and triangular conditions ($n\geq60$ cells for each condition). (**g**) Fraction of cells that were polarized in untreated, mock-, EB1-, LIC1-, LIC2- and Par3-siRNA-treated cells plated on triangular micropatterns ($n\geq60$ cells for each condition). (**h**) Extents of polarization of untreated, mock-, EB1-, LIC1-, LIC2- and Par3-siRNA-treated cells plated on triangular micropatterns ($n\geq60$ cells for each condition).

EB1 and LIC1 regulate MTOC positioning and polarization in both single and confluent cells

Next, we set out to identify proteins that are involved in the polarization pathway of, but not limited to, single cells. Because the above results demonstrated that microtubules affect MTOC positioning and, to a lesser extent, nuclear positioning, we examined microtubule end-binding protein 1 (EB1), which shows a comet-like distribution in confluent and triangular fibroblasts (Fig. 5a). Previous results have shown that wound-edge cells expressing a mutated form of Apc that lacks EB1-binding sites fail to reorient their centrosomes and polarize (Etienne-Manneville and Hall, 2003). EB1 could play a role in the anchoring of microtubules at the plasma membrane during polarization events, so we hypothesized that EB1 would be essential for the establishment of cell polarity in both single and confluent cells.

We used siRNA to deplete EB1 by ~50% (Fig. 4b). EB1-depleted cells showed a dramatically increased MTOC–cell centroid distance in confluent cells (+86±12%, $P<0.001$) and in single cells plated on circular (+54±12%, $P<0.001$) and triangular (+31±10%, $P<0.05$) micropatterns (Fig. 4d, black bars; 4e, top panel); depletion of EB1 had no significant effect on the nucleus–cell centroid distance in all conditions (Fig. 4d, gray bars; 4f, top panel). Interestingly, EB1 depletion reversed the polarization of triangular cells to a significant extent in terms of both the fraction of cells that were polarized ($P<0.01$; Fig. 4g) and extent of horizontal polarization ($P<0.05$; Fig. 4h), such that their MTOCs were more likely to be found to the right of a line vertically bisecting the nucleus, toward the sharp end of the cell.

Because LIC2 depletion did not affect MTOC positioning in single cells, we next examined dynein light intermediate chain 1 (LIC1), to determine if this related isoform played a role in MTOC positioning and polarization. Previous research has identified that distinct LIC isoforms, namely LIC1 and LIC2, define unique subclasses of cytoplasmic dynein with particular functions. LIC1-containing dynein, but not LIC2-containing dynein, binds to the centrosomal protein pericentrin (Tynan et al., 2000). Visualization of LIC1 in confluent fibroblasts revealed bright perinuclear puncta, corroborating the presence of LIC1 at the centrosome (Fig. 5b, upper panels). Discrete roles for LIC1 and LIC2 in membrane-trafficking processes have also been identified, thus making it plausible that LIC1 and LIC2 could play different roles in cell polarization in a cell confluence-dependent manner as well. Both light intermediate chains mutually bind the heavy chain of dynein (Tynan et al.,

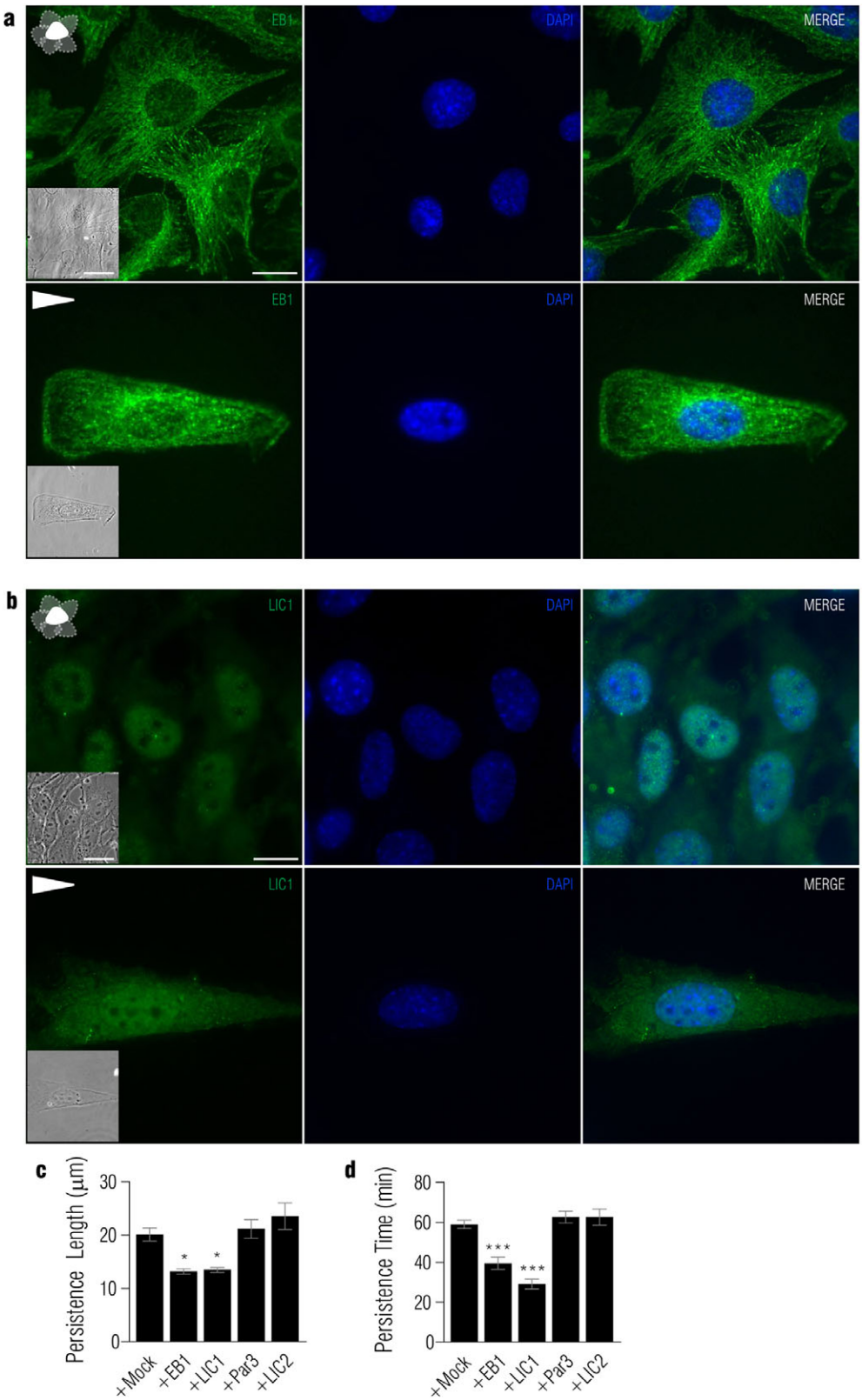

Fig. 5. EB1 or LIC1 depletion impairs directional cell motility. (**a**) Immunofluorescence of EB1 (green) and the nucleus (blue) in confluent (top) and triangular (bottom) cells. Scale bar: 10 μm. Insets: corresponding phase-contrast images (bottom left). Scale bar: 20 μm. (**b**) Immunofluorescence of LIC1 (green) and the nucleus (blue) in confluent (top) and triangular (bottom) cells. Scale bar: 10 μm. Insets: corresponding phase-contrast images (bottom left). Scale bar: 20 μm. (**c**,**d**) Persistence length (c) and time (d) during the migration of single MEFs transfected with mock, EB1, LIC1, Par3 and LIC2 siRNAs (n=15 cells for each condition).

2000), but previous work has shown that LIC1 depletion does not affect centrosome reorientation in wound-edge fibroblasts (Schmoranzer et al., 2009). We wanted to test the role of LIC1 in single-cell polarization. LIC1 levels were specifically reduced by ~60% upon siRNA treatment (Fig. 4b). Interestingly, similar to EB1 knockdown, knockdown of LIC1 significantly increased the MTOC–cell centroid distance in confluent cells (+107±12%, $P<0.001$) and in circular (+47±11%, $P<0.01$) and triangular cells (+28±7%, $P<0.05$; Fig. 4d, black bars; 4e, upper middle panel), whereas the position of the nucleus was unaffected in all conditions (Fig. 4d, gray bars; 4f, upper middle panel). The polarization of these cells was reversed as well, with significant reductions in both the fraction of cells that were polarized ($P<0.05$; Fig. 4g) and extent of horizontal polarization ($P<0.01$; Fig. 4h).

A similar reversal of polarization was detected in cells treated with lithium chloride, which globally inhibits GSK-3β (Fig. 6d,e). The spatial inactivation of GSK-3β is required to maintain polarization in migrating astrocytes (Etienne-Manneville and Hall, 2003). Lithium chloride treatment did not significantly affect the net distance of the MTOC or the nucleus from the cell centroid in triangular cells (Fig. 6a, lower panel; 6b,c), suggesting that global GSK-3β inhibition caused a directional shift of the MTOC from the blunt end of the cell towards the sharp end. GSK-3β inhibition caused a significant increase in the MTOC–cell centroid distance in circular cells, but did not significantly affect the position of the nucleus (Fig. 6a, upper panel; 6b,c). These results demonstrate that although certain proteins previously implicated in the cellular polarization pathway are not necessarily required for single-cell polarization, namely LIC2 and Par3, the activity of several other proteins are required to maintain polarization in single cells, including EB1, LIC1 and GSK-3β.

EB1 or LIC1 depletion impairs directional cell motility

The inability of cells to polarize on triangular micropatterns suggested that their mobility would also be impaired; we performed a single-cell motility assay to directly test this hypothesis. Following siRNA transfection, MEFs were imaged for 14 hours and tracked, and persistence length and time of migration, representing the curvilinear distance and time a cell travels before significantly deviating from a straight trajectory, respectively, were calculated for each cellular population. Depletion of EB1 or LIC1 significantly reduced both cellular persistence length ($P<0.05$; Fig. 5c) and persistence time ($P<0.001$; Fig. 5d) relative to mock-transfected cells, whereas depletion of Par3 or LIC2 had no significant effect. These results confirm that EB1 and LIC1, but not Par3 and LIC2, are essential for both single-cell polarization and directional motility and reinforce the predictive power of the triangular polarization assay as an effective tool for the assessment of functional cell motility.

Nuclear lamins and the nucleo-cytoskeletal connection are essential for MTOC and nucleus positioning

In addition to examining the effect of cytoskeletal binding partners at the cell periphery, we sought to determine the role of proteins located near the opposite end of cytoskeletal filaments, or centrally, in MTOC and nucleus positioning. Actin filaments can polymerize and bind to a multitude of proteins and structures within the cell, including other actin filaments, through nucleation involving the Arp2/3 complex (Goley and Welch, 2006), the plasma membrane through the cadherin–catenin complex in contacting cells (Weis and Nelson, 2006), and the nuclear envelope through LINC complex proteins (Khatau et al., 2009; Razafsky and Hodzic, 2009), among others. In the latter case, actin microfilaments can directly or indirectly bind outer nuclear membrane nesprin isoforms (Wilhelmsen et al., 2005; Zhen et al., 2002), which in turn interact with Sun proteins localized to the inner nuclear membrane (Stewart-Hutchinson et al., 2008). Inside the nucleus, Sun proteins bind nuclear lamins (Crisp et al., 2006; Worman and Gundersen, 2006), and current models suggest that this protein bridge physically connects the interior of the nucleus to the cytoskeleton of the cell (see Fig. 8a). Thus, we hypothesized that this nucleo-cytoskeletal link would play a significant role in positioning both the nucleus and, through the microtubule-mediated MTOC–nucleus connection (Salpingidou et al., 2007), the MTOC of the cell.

To test this hypothesis by perturbing nucleo-cytoskeletal connections, we plated A-type-lamin-deficient fibroblasts ($Lmna^{-/-}$ MEFs), on circular and triangular micropatterns and assessed the positions of MTOCs and nuclei. LINC complex proteins are abnormally positioned in $Lmna^{-/-}$ MEFs (Hale et al., 2008) and the MTOC–nucleus distance is abnormally large (Hale et al., 2008; Lee et al., 2007; Salpingidou et al., 2007). Therefore these cells were a suitable model to assess the role of nucleo-cytoskeletal connections. We verified that the MTOC–nucleus distance was significantly increased in circular $Lmna^{-/-}$ fibroblasts (0.9±0.2 μm) relative to wild-type fibroblasts (0.3±0.1 μm; $P<0.001$; Fig. 7a), although interestingly, when plated on triangular micropatterns, this distance increased only slightly (from 0.2±0.1 μm in wild type to 0.3±0.1 μm in $Lmna^{-/-}$) and not significantly ($P>0.05$). In $Lmna^{-/-}$ fibroblasts plated on circular micropatterns, the nucleus–cell centroid distance increased significantly (+70±10%; $P<0.001$; Fig. 6f, gray bars; 6h) relative to wild-type circular fibroblasts. The MTOC–cell centroid distances increased significantly as well (+25±9%; $P<0.05$; 6f, black bars; 6g), although not as dramatically. Although both the MTOC– and nucleus–cell centroid distances increased in triangular $Lmna^{-/-}$ fibroblasts relative to wild-type fibroblasts (Fig. 6f, lower panel; 6g,h), the increases were not significant ($P>0.05$). Nevertheless, triangular $Lmna^{-/-}$ fibroblasts failed to polarize towards the blunt end, as indicated by the fraction of cells that were polarized (Fig. 6i) and the extent of polarization (Fig. 6j). These results suggest that lamins, and the nucleo-cytoskeletal connections they maintain, play a role in both MTOC and nucleus positioning in a shape-dependent manner.

Discussion

Much progress has been made in identifying the proteins and pathways that regulate MTOC and nuclear positioning in polarized astrocytes and fibroblasts through the scratch-wound assay. This assay is useful to study large numbers of cells that polarize at a wound edge, but requires cells to be in contact with one another. However, neither directed cell migration (Friedl, 2004) nor cell polarization, as demonstrated here, absolutely require cell–cell contacts. In vivo, mesenchymal cells, such as astrocytes and fibroblasts, do not function within confluent cellular structures. Instead, they polarize and migrate as single cells. Moreover, cellular polarization could depend on intrinsic cell shape, which is not controlled in the scratch-wound assay. This raises the following crucial question: do the previously identified molecular pathways that seemingly govern cell

polarization apply to the more physiological case of single-cell polarization? We addressed this question by characterizing single fibroblasts on protein micropatterns, allowing us to systematically assess the role of cell shape and specific proteins in governing the positioning of the MTOC and nucleus as well as polarization in single cells.

Although several studies have indicated that the MTOC is located at the cell center in both quiescent and polarized states (Burakov et al., 2003; Gomes et al., 2005), our results suggest that the position of the MTOC depends largely on cell shape. Our results have predominantly been determined from examining the MTOC and nucleus positions at a fixed time point of 3 hours

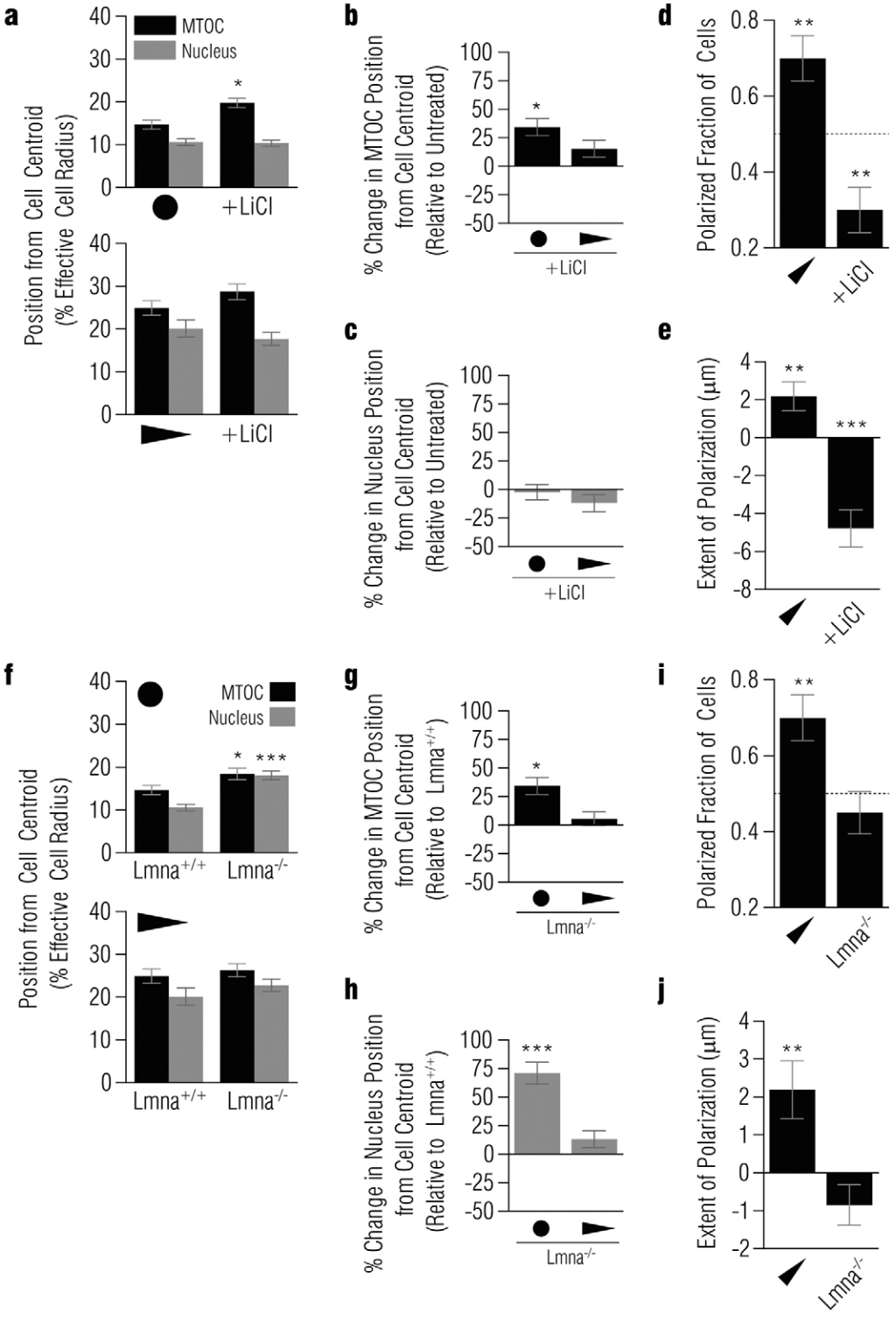

Fig. 6. See next page for legend.

post-plating, but additional live-cell experiments with confluent MEFs stably transfected with CETN2–RFP and incubated with DRAQ5 to visualize the MTOC and nucleus, respectively, confirmed that average distances of the MTOC and the nucleus from the cell centroid over a 5-hour time period (after which they were plated) did not significantly differ from average distances determined in fixed cells (supplementary material Fig. S2c,d), suggesting that the 3-hour 'snapshot' provides a representative view of the MTOC and nucleus position. It is also important to note that whether the MTOC is located at the cell center or not depends on how a cell 'center' is defined. When the cell center is defined as a circular region 12 μm in diameter (20% of the cell diameter) centered on the geometric center of the cell, MTOCs are only centered in a majority of circular and confluent cells, but not in triangular or in sparse cells. Furthermore, MTOCs are most off-centered in triangular cells, which are polarized by this shape alone. On average, MTOCs are found ~7.5 μm away (25% of the effective radius of the cell) from the cell centroid in triangular cells. By contrast, MTOCs are mostly centered in circular cells, which because of their underlying symmetrical micropattern, are not polarized in any particular direction. These results suggest that MTOC centering in cells depends crucially on cell shape and that the MTOC is repositioned away from the cell centroid during polarizing events, to a position between the leading edge of the cell and its nucleus.

Fig. 6. GSK-3β and A-type lamins in MTOC and nucleus positioning. (**a**) Average distances of the MTOC (black) and nucleus (gray) from cell centroid in untreated and LiCl-treated circular (top) and triangular (bottom) cells. Asterisks indicate significant differences between LiCl-treated and untreated cells using a one-way ANOVA followed by Dunnett's multiple comparison test ($n \geq 60$ cells for each condition). (**b**,**c**) Percent change in the distances of the MTOC (b) and nucleus (c) from the cell centroid upon LiCl treatment relative to that in untreated circular and triangular cells. Asterisks indicate significant differences between LiCl-treated and untreated cells using a one-way ANOVA followed by Dunnett's multiple comparison test ($n \geq 60$ cells for each condition). (**d**) Fractions of cells that were polarized in untreated and LiCl-treated cells plated on triangular micropatterns. Asterisks indicate that a population is significantly polarized compared with an unpolarized population-based theoretical mean of 0.5, using a one sample *t*-test ($n \geq 60$ cells for each condition). (**e**) Extents of polarization of untreated and LiCl-treated cells plated on triangular micropatterns. Asterisks indicate that a population is significantly polarized, compared with an unpolarized population-based theoretical mean of 0.0 using a one-sample *t*-test ($n \geq 60$ cells for each condition). (**f**) Average distances of the MTOC (black) and nucleus (gray) from the cell centroid in wild-type and *Lmna*$^{-/-}$ circular (top) and triangular MEFs (bottom). Asterisks indicate significant differences between *Lmna*$^{-/-}$ and wild-type fibroblasts using a one-way ANOVA followed by Dunnett's multiple comparison test ($n \geq 60$ cells for each condition). (**g**,**h**) Percentage change in the distances of the MTOC (g) and nucleus (h) from the cell centroid in *Lmna*$^{-/-}$ fibroblasts relative to wild-type circular and triangular fibroblasts. Asterisks indicate significant differences between *Lmna*$^{-/-}$ and wild-type fibroblasts using a one-way ANOVA followed by Dunnett's multiple comparison test ($n \geq 60$ cells for each condition). (**i**) Fractions of wild-type and *Lmna*$^{-/-}$ fibroblasts that were polarized after plated on triangular micropatterns. Asterisks indicate that wild-type fibroblasts were significantly polarized, compared with an unpolarized population-based theoretical mean of 0.5, using a one sample *t*-test ($n \geq 60$ cells for each condition). (**j**) Extents of polarization of wild-type and *Lmna*$^{-/-}$ fibroblasts plated on triangular micropatterns. Asterisks indicate that a population is significantly polarized, compared with an unpolarized population-based theoretical mean of 0.0 using a one-sample *t*-test ($n \geq 60$ cells for each condition).

Our quantitative observations are in disagreement with the model in which the MTOC remains centered in the cell during wound-edge polarization events (Gomes et al., 2005). Instead, our results demonstrate that during single-cell polarization events, the MTOC is repositioned to an off-centered position towards the leading edge of the cell, consistent with previous observations in other scratch-wound studies (Etienne-Manneville and Hall, 2001; Palazzo et al., 2001). Our experiments, however, do support a model in which the nucleus is relocated rearward to an off-centered position during polarization events in an actin- and myosin II-dependent manner (Gomes et al., 2005). These oppositely directed movements thus generate the morphology in which the MTOC is positioned between the leading edge and the nucleus in single polarized cells. Our results indicate that the mechanisms driving cell polarization depend on whether a cell is isolated or in contact with other cells, and that cell confluence must be considered when assessing factors that affect cell polarization.

Cytoskeletal interference experiments carried out on triangular micropatterns indicate that actin, myosin II, active myosin light chain kinase, microtubules and microtubule dynamics are all required for single-cell polarization. Nevertheless, the manner in which these proteins regulate MTOC and nucleus positioning crucially depends on both cell shape and cell confluence. Studies suggest that microtubules exclusively affect MTOC positioning, whereas actin and myosin affect only nucleus positioning (Gomes et al., 2005). Our results in confluent cells agree with this framework to the extent that microtubules and microtubule dynamics strictly affected MTOC positioning and not nucleus positioning. However, in confluent cells treated with either an actin-depolymerizing agent, a myosin II inhibitor, or an MLCK inhibitor, perturbations in nuclear positioning were coupled to changes in MTOC positioning, possibly due to the tight connection between these two organelles (Crisp et al., 2006; Hale et al., 2008; Salpingidou et al., 2007). Furthermore, the role of actin, myosin II, myosin light chain kinase and microtubules depend closely on the conditions in which the cells are studied. For example, MTOCs became largely off-centered in circular cells upon microtubule depolymerization, whereas MTOCs in identically treated sparse cells showed little change in MTOC positioning. Additionally, the effect of actin depolymerization and myosin II inhibition on MTOC and nuclear positioning was relatively weak in confluent, circular and triangular cells relative to sparse cells. Although this can be attributed to a less significant role of actomyosin contractility in positioning the MTOC and nucleus in these conditions, it could also indicate weaker actin retrograde flow, particularly in confined micropatterned cells. Altogether, these results suggest that although the cytoskeletal proteins studied here are essential for single-cell polarization, there are many mechanisms by which these proteins regulate MTOC and nucleus positioning, and that these mechanisms depend on both cell shape and confluence. This finding not only has implications in unraveling the biological intricacies of organelle positioning, but also highlights the importance of mimicking in vivo conditions to the greatest extent that in vitro assays will allow in order to generate results that can be applied to physiological cellular conditions.

It is possible that only the subset of actin fibers that are tightly connected to the nuclear envelope through LINC complexes and form the perinuclear actin cap (Khatau et al., 2009; Khatau et al., 2010) mediate the actomyosin-based positioning of the nucleus in single adherent cells. Indeed, the depolymerization of F-actin, the

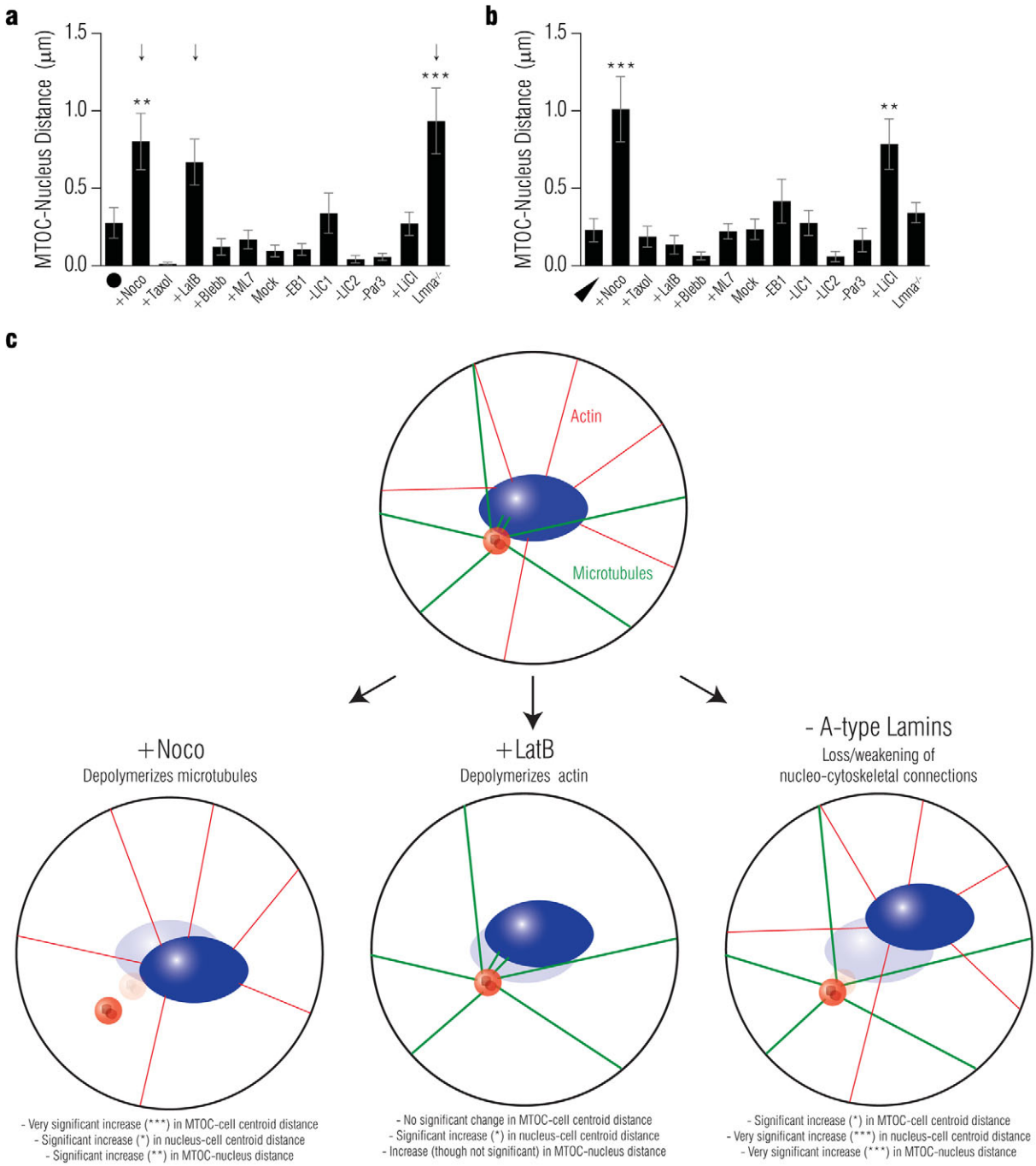

Fig. 7. Importance of the MTOC–nucleus connection. (**a**,**b**) MTOC–nucleus distance, defined as the distance between the nuclear rim and the MTOC centroid, in circular (a) and triangular (b) fibroblasts for several conditions. Asterisks indicate significant differences between indicated population and untreated cells, using a one-way ANOVA followed by Dunnett's multiple comparison test. Arrows indicate specific conditions described in c ($n \geq 60$ cells for each condition). (**c**) A simplified diagram showing the effects of nocodazole treatment, latrunculin B treatment and loss of A-type lamins on MTOC and nucleus positioning in circular fibroblasts. Top: in an untreated, wild-type fibroblast, three main connections are intact within the cell that function to position the MTOC and nucleus: (1) microtubules (green) connect the MTOC to the plasma membrane; (2) actin connects the nucleus to the plasma membrane; and (3) short microtubule tethers connect the MTOC and nucleus. Bottom: upon microtubule depolymerization, the first and third connections are eliminated, causing a very significant increase in the MTOC–cell centroid distance, a significant increase in the nucleus–cell centroid distance and a significant increase in the MTOC–nucleus distance. Note that positional changes are exaggerated slightly to allow easier visualization of trends. Upon actin depolymerization, only the second connection is eliminated, causing no significant change in the MTOC–cell centroid distance, a significant increase in the nucleus–cell centroid distance, and a subtle, though non-significant, increase in the MTOC–nucleus distance. Upon loss of A-type lamins in *Lmna*$^{-/-}$ fibroblasts, the third connection is compromised, causing a significant increase in the MTOC–cell centroid distance, a very significant increase in the nucleus–cell centroid distance and a very significant increase in the MTOC–nucleus distance. Taken together, these results demonstrate the importance of nucleo-cytoskeletal connections in regulating the position of both the MTOC and nucleus.

a

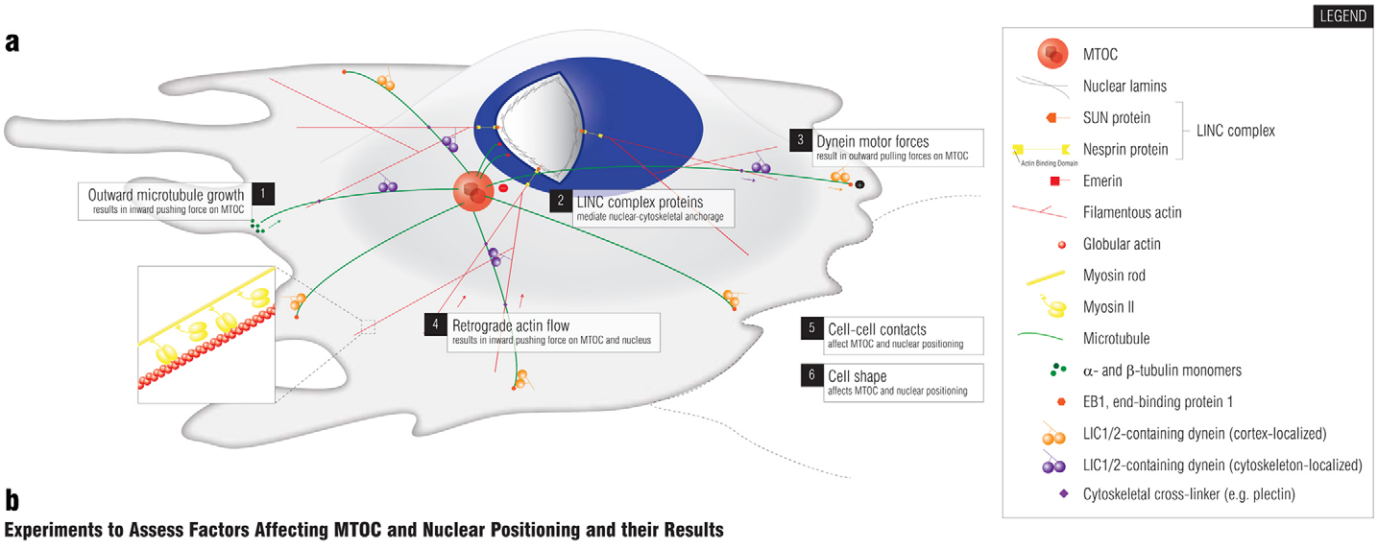

b

Experiments to Assess Factors Affecting MTOC and Nuclear Positioning and their Results

Intervention	Action	Forces Hypothetically Affected	Results
Cell confluence	Cells plated at low and high density to assess effect of cell-cell contacts	1, 3, 4, 5, 6	▪ Comparing untreated sparse and confluent cells, the presence of cell-cell contacts correlated with more centered MTOCs (Fig. 1G) ▪ Comparing untreated confluent to circular cells, the presence of cell-cell contacts was associated with zipper-like structures of Par3 along cell-cell contacts (Fig. 4A)
Cell shape	Cell shape control via protein micropatterning	1, 3, 5, 6	▪ Relative to symmetric, non-polarizing shapes (e.g. circles), polarizing shapes (e.g. isosceles triangles) were associated with more off-centered MTOCs and nuclei (Fig. 1C-G)
+LatB	Depolymerizes actin	4	▪ Actin depolymerization centered MTOCs of sparse cells, off-centered nuclei of circular cells, and abrogated polarization of triangular cells (Fig. 2B-F)
+Blebb	Inhibits myosin II	4	▪ Myosin II inhibition centered both MTOCs and nuclei of sparse cells and abrogated polarization of triangular cells (Fig. 2B-F)
+ML7	Inhibits myosin light chain kinase	4	▪ MLCK inhibition centered MTOCs of sparse cells, off-centered nuclei of circular cells, and abrogated polarization of triangular cells (Fig. 2B-F)
+Noco	Depolymerizes microtubules	1, 3	▪ Microtubule depolymerization off-centered MTOCs of confluent, circular, and triangular cells; centered nuclei of sparse cells; off-centered nuclei of circular cells; increased the MTOC-nucleus distance in both circular and triangular cells; and abrogated polarization of triangular cells (Fig. 3B-F, 7A-B)
+Taxol	Inhibits microtubule dynamics	1	▪ Inhibition of microtubule dynamics off-centered nuclei of confluent cells and abrogated polarization of triangular cells (Fig. 3B-F)
-EB1 (siRNA)	EB1 depletion	1, 3	▪ EB1 depletion off-centered MTOCs of confluent, circular, and triangular cells; abrogated polarization of triangular cells; and reduced cells' persistence length and time (Fig. 4D-H, 5B-C)
-LIC1 (siRNA)	LIC1 depletion	3	▪ LIC1 depletion off-centered MTOCs of confluent, circular, and triangular cells; abrogated polarization of triangular cells; and reduced cells' persistence length and time (Fig. 4D-H, 5B-C)
-LIC2 (siRNA)	LIC2 depletion	3	▪ LIC2 depletion off-centered MTOCs only in confluent cells and did not affect polarization of triangular cells (Fig. 4D-H)
-Par3 (siRNA)	Par3 depeletion	3	▪ Par3 depletion off-centered MTOCs only in confluent cells and did not affect polarization of triangular cells (Fig. 4D-H)
+LiCl	GSK-3β inhibition	1, 3	▪ GSK-3β inhibition off-centered MTOCs of circular cells, increased the MTOC-nucleus distance in triangular cells, and abrogated polarization of triangular cells (Fig. 6A-E, 7B)
Lmna$^{-/-}$	A-type nuclear lamins depleted	2	▪ Depletion of A-type nuclear lamins off-centered both MTOCs and nuclei in circular cells, increased the MTOC-nucleus distance in circular cells, and abrogated polarization of triangular cells (Fig. 6F-J, 7A)

Fig. 8. Forces and cellular conditions that affect MTOC and nuclear positioning. (**a**) A cartoon of the primary and hypothesized forces acting on the MTOC and nucleus to regulate their position. (**b**) Design and results of experiments performed using drugs, siRNA and gene knockouts to manipulate specific forces acting on the MTOC and nucleus.

inhibition of MLCK and/or Rho kinase using low concentrations of pharmacological inhibitors, the disruption of the LINC complexes, and lamin A/C deficiency all specifically and substantially reduce the formation of the perinuclear actin cap (Khatau et al., 2009). Nevertheless, more work is needed to establish the direct role of the perinuclear actin cap in nuclear positioning.

Experiments with *Lmna*$^{-/-}$ cells highlight the importance of the nucleus–MTOC connection in regulating the positions of both the MTOC and nucleus. Comparing results between nocodazole-treated,

latrunculin-B-treated and *Lmna*$^{-/-}$ fibroblasts on circular micropatterns demonstrates that nucleo-cytoskeletal connections are not simply passive tethers, but rather, they function as either an anchoring or force-generating mechanism (possibly involving microtubule motor proteins) that regulates both MTOC and nucleus positioning (Fig. 6c). *Lmna*$^{-/-}$ fibroblasts plated on triangular micropatterns failed to polarize towards the blunt end of the shape, consistent with previous polarization defects observed in wound-healing and shear assays (Hale et al., 2008; Lee et al., 2007). *Lmna*$^{-/-}$ fibroblasts are a mouse model of the human laminopathic disease autosomal-dominant Emery–Dreifuss muscular dystrophy, these results reinforce the importance of lamins in maintaining cell health and pinpoint a possible mechanism by which these cells fail to polarize and contribute to manifestation of disease.

Specific protein depletion combined with polarization experiments revealed that Par3 and LIC2 are required for cell polarization in scratch-wound assays (Schmoranzer et al., 2009), but are not required for the polarization of single cells, as demonstrated here. Furthermore, depletion of these proteins does not affect single-cell motility as assessed by cellular persistence length and time of migration. MTOC positioning in circular and triangular Par3- and LIC2-depleted cells was unaffected relative to mock-transfected cells, and accordingly, Par3- and LIC2-depleted cells polarized on triangular micropatterns. These results suggest that although Par3 and LIC2 are required for confluent cell polarization, they are not required for MTOC repositioning in single-cell polarization.

Par3- and LIC2 depletion affected MTOC positioning in a cell–cell contact-dependent manner, but depletion of either EB1 or LIC1 affected MTOC positioning in both confluent and single cells. Furthermore, depletion of either EB1 or LIC1 prevented single cells from polarizing towards the blunt end of the triangle and in single-cell motility experiments, depletion of either protein reduced persistence length and time of migration. Interestingly, these cells showed a preferential polarization toward the sharp end of the triangle, which was also detected in cells treated with LiCl to globally inhibit GSK-3β. Although this could be due to the roles of these proteins in regulating microtubule length (which is perturbed upon protein depletion), further experiments are required to investigate this phenomenon. It is important to note that although the MTOC–cell centroid distance in nocodazole-treated cells on triangular microarrays increased while nucleus position was largely unaffected, a reverse in polarization was not observed. This is most probably due to the fact that microtubules were depolymerized, and thus, a driving force to reposition the MTOC to the right of the nucleus was not present in these cells, as it was in cells with either reduced EB1 expression, reduced LIC1 expression, or globally inhibited GSK-3β.

The requirement of specific proteins for both confluent and single-cell polarization and the conditional requirement of other proteins for cell polarization suggest a Cdc42-dependent polarization pathway that diverges based on the presence of cell–cell contacts. The polarizing cue in single cells is the asymmetric presentation of ECM proteins to the basal surface of the cell, whereas in collective cell polarization, the trigger is either loss of cell–cell contact or an activation signal released by damaged cells at the wound edge (Berzat and Hall, 2010). Abolition of polarization due to global inhibition of GSK-3β suggests that single-cell polarization does indeed follow the Cdc42–Par6–PKCζ pathway, and that divergence must be downstream of spatial GSK-3β inhibition in this pathway. Furthermore, as EB1 and LIC1 are required for proper MTOC positioning in both single and confluent cells, this divergence most probably occurs downstream of microtubule anchoring at the plasma membrane. Recruitment and activation of the dynein–dynactin motor complex is thought to then create pulling forces at the plasma membrane that drives MTOC positioning. Divergence of the polarization pathway most probably occurs at this point, where LIC1- and LIC2-containing dynein performs functions with similar outcomes but under different conditions; LIC1-containing dynein is involved in single-cell MTOC repositioning, whereas LIC-2-containing dynein is involved in confluent cell MTOC repositioning. This MTOC repositioning, coupled with actin- and myosin II-dependent rearward movement of the nucleus, thus generates the polarized morphology of both single and confluent cells.

Future studies directed towards elucidating cell polarization pathways must consider the variables of cell–cell contact and cell shape, as our studies demonstrate that these two extracellular guidance cues have a significant effect on the cellular response to drugs affecting the cytoskeleton, and that the proteins involved in orchestrating cellular polarization depend on the presence of cell–cell contacts. Here we have implemented a SMRT analysis system to address these variables in an attempt to bridge gaps in the understanding of cell polarization that have arisen because of assay variability. We have identified two proteins, EB1 and LIC1, which are essential for the generation of functional single-cell polarization. We have summarized our experimental design and findings in Fig. 8b. Further studies will be required to understand more precisely how intracellular communication activates a particular branch of the divergent polarization pathway in cells in order to carry out an efficient response to a polarizing stimulus, as well as whether other proteins are specifically involved in each branch of the polarization response. A more complete understanding of these intricacies of the generation and maintenance of polarization in cells will contribute to our comprehension of the biology and mechanics behind aberrant cell migration in human cancers and diseases.

Materials and Methods

Cell culture and drug treatments

Mouse embryonic fibroblasts (MEFs) were cultured in DMEM (Invitrogen, Carlsbad, CA) supplemented with 10% fetal bovine serum (FBS; Hyclone, Logan, UT) and 100 IU penicillin and 100 μg streptomycin (Sigma, St Louis, MO) and maintained at 37℃ in a humidified, 5% CO_2 environment. For sparse and confluent cell experiments, cells were seeded at $\sim 2 \times 10^3$ cells/ml and $\sim 1 \times 10^4$ cells/ml, respectively, on 35-mm glass bottom dishes (MatTek, Ashland, MA) coated with 50 μg/ml fibronectin (BD Biosciences, Sparks, MD). Cells were seeded at $\sim 2 \times 10^3$ cells/ml on fibronectin micropatterned dishes; medium was refreshed 1 hour after plating to remove excess cells. For siRNA transfection and immunoblotting experiments, cells were seeded at $\sim 1 \times 10^4$ cells/ml on 10-cm cell culture dishes (Corning, Corning, NY). *Lmna*$^{-/-}$ MEFs were generated by targeted disruption of the lamin A/C gene (Sullivan et al., 1999), provided by Colin Stewart (Institute of Medical Biology, Singapore), and cultured as described above.

The microtubule destabilizer nocodazole (Sigma), the microtubule stabilizer Taxol (also known as paclitaxel; Invitrogen), the F-actin disassembly drug latrunculin B (Sigma), the non-muscle myosin II inhibitor (–)-blebbistatin (Sigma), the myosin light chain kinase inhibitor ML-7 (Sigma), and the GSK-3β inhibitor LiCl (Sigma), were diluted from stock using culture medium. Nocodazole was used at a final concentration of 3.3 μM. Taxol was used at a final concentration of 1 μM. Latrunculin B was used at a final concentration of 0.5 μM. ML-7 was used at a final concentration of 20 μM. Blebbistatin was used at a final concentration of 25 μM. LiCl was used at a final concentration of 20 mM. Before fixation, 3 hours after seeding, cells were incubated with each drug for 30 minutes, except for the LiCl treatment, when cells were treated for 1 hour.

siRNA depletion and immunoblotting

MEFs were co-transfected with validated Stealth^{TM} RNAi siRNA oligonucleotides (Invitrogen) specific to each protein target and Block-iT Fluorescent Oligo (Invitrogen) for fluorescence indication of oligomer uptake using Lipofectamine RNAiMAX (Invitrogen) according to the manufacturer's protocol. The sequences used were as follows: EB1, 5′-CAUUGCAACACAGAGGACUACUGCA-3′; LIC1 5′-GGUGGAGAAGGACGCAGUGUUUAUU-3′; LIC2, 5′-GACAUGUCUCGACCUUGGACGAUAA-3′; Par3, 5′-GACCCAGCUUUAACUGGCCUUUCCA-3′. BLAST searches confirmed that each sequence specifically targeted the intended protein. Nonsilencing controls (mock transfections) were performed using Stealth^{TM} RNAi siRNA Negative Control (Medium GC, Invitrogen), which is not homologous to anything in the vertebrate transcriptome and has been confirmed to not induce a stress response.

Whole cell lysates were prepared on ice with protease inhibitors and phenylmethanesulfonylfluoride (PMSF; Roche, Basel, Switzerland) in NP-40 lysis buffer from cultures grown on 10-cm tissue culture dishes. Lysates were centrifuged at 18,000 ***g*** at 4℃ for 10 minutes. Protein concentration of supernatants was measured using a Bradford assay and samples were diluted accordingly in order to load samples at equal concentrations. Protein samples were then boiled at 100℃ for 5 minutes in 1× Laemmli buffer, resolved by 12.5% SDS-PAGE at 100 V (constant voltage) for 100 minutes, and then transferred to nitrocellulose membranes (Invitrogen) in Towbin buffer at 300 mA (constant amperage) for 90 minutes. Protein transfer was confirmed with Ponceau S (Sigma) staining. Membranes were then blocked with 5% BSA for 1 hour at 4℃, probed with the appropriate primary antibody diluted in 1× Tris-buffered saline containing 0.1% Tween 20 (TBST) overnight at 4℃, washed with 1× TBST, probed with anti-actin horseradish peroxidase (HRP; Santa Cruz Biotechnology, Santa Cruz, CA) for 2 hours at room temperature (RT) as a loading control, and blotted with the appropriate HRP-conjugated secondary antibody diluted in 1× TBST for 2 hours at RT. Membranes were then developed using SuperSignal West Dura Extended Duration Substrate (Thermo Scientific, Rockford, IL) and imaged with a ChemiDoc XRS+ System (Bio-Rad, Hercules, CA). Protein levels were quantified using Adobe Photoshop (Adobe, San Jose, CA).

The following antibodies were used for immunoblotting: mouse monoclonal anti-EB1 antibody at 1:1000 (BD Biosciences), rabbit polyclonal anti-Par3 antibody at 1:1000 (Millipore, Billerica, MA), rabbit polyclonal anti-pan-LIC antibody at 1:500 (kindly provided by Richard Vallee, Columbia University, NY), which detects both LIC1 and LIC2 (Tynan et al., 2000), and goat anti-mouse and goat anti-rabbit IgG–HRP secondary antibodies (Santa Cruz Biotechnology).

Immunofluorescence microscopy

Cells were fixed 3 hours after plating and stained as previously described (Hale et al., 2009). Specifically, cells were fixed with either ice-cold methanol for 3 minutes or 2.5% paraformaldehyde (Electron Microscopy Sciences, Hatfield, PA) for 10 minutes, washed with 1× phosphate-buffered saline (PBS) at room temperature (RT), and permeabilized with 0.1% Triton X-100 for 10 minutes. PBS supplemented with goat serum (10%; Sigma) was used to block nonspecific binding, after which cells were incubated with primary and secondary antibodies, respectively, at the appropriate dilutions for 1 hour each at RT. For α-tubulin and γ-tubulin staining, cells were incubated with a mouse monoclonal anti-α-tubulin antibody (Abcam, Cambridge, MA) and a rabbit polyclonal anti-γ-tubulin antibody (Abcam), respectively, at 1:500 dilutions, and subsequently incubated with Alexa Fluor 488 goat anti-mouse and Alexa Fluor 568 goat anti-rabbit secondary antibodies (Invitrogen), respectively, at 1:200 dilutions. For EB1 staining, cells were incubated with a mouse monoclonal anti-EB1 antibody (BD Biosciences) at 1:100 dilution and subsequently incubated with Alexa Fluor 488 goat anti-mouse secondary (Invitrogen) at 1:200 dilution. For LIC1 staining, cells were incubated with a goat polyclonal anti-LIC1 antibody (Santa Cruz Biotechnology) at 1:50 dilution and subsequently incubated with Alexa Fluor 488 rabbit anti-goat secondary (Invitrogen) at 1:200 dilution. Nuclear DNA was stained during secondary treatment using 300 nM DAPI (Invitrogen) or 0.5 μM DRAQ5 (Cell Signaling, Danvers, MA). For cells treated with latrunculin B, blebbistatin or ML-7, paraformaldehyde was used as a fixative and actin was stained during secondary treatment using Alexa-Fluor-488–phalloidin (Invitrogen) at 1:40 dilution.

Cells were then cured in ProLong Gold antifade reagent (Sigma) and covered with a coverslip before visualization. Phase-contrast and fluorescence micrographs were collected using a Cascade 1K CCD camera (Roper Scientific, Tucson, AZ), mounted on a Nikon TE2000 microscope with either a 10× Plan Fluor (NA 0.3, Nikon, Melville, NY) or a 60× Plan Fluor lens (NA 1.4, Nikon) controlled by Metavue (Universal Imaging, West Chester, PA). Images were digitally overlaid using Metamorph (Universal Imaging).

Protein micropatterning

A custom mask with circular and triangular shapes was generated using Adobe Illustrator (Adobe), printed on a transparency at high resolution (Pageworks, Cambridge, MA), and used to generate a master mold (Khatau et al., 2009). Briefly, a silicon wafer was rinsed with water and ethanol and then baked at 95℃ for 2 minutes. SU-8 2010 photoresist (MicroChem, Newton, MA) was then spun onto the silicon at 4000 rpm to achieve a thickness of ~7.5 μm. The wafer was then baked at 95℃ for 3 minutes, after which it was exposed to UV light through the mask, post-baked at 115℃ for 5 minutes, and developed for 2 minutes. The wafer was then rinsed with isopropanol and a gentle stream of nitrogen. Next, the wafer was silanized with octadecyltrichlorosilane (Sigma) heated to 30℃ for 5 minutes to facilitate removal of polydimethylsiloxane (PDMS) from the master wafer in subsequent steps. Following silanization, the wafer was baked at 110℃ for 5 minutes and then cleaned stepwise with hexane, distilled water and ethanol for 5 minutes each in an ultrasonic bath (Holgerson et al., 2005). PDMS (Corning) was prepared and degassed for 30 minutes before being poured over the master patterns and allowed to cure at RT for 24 hours. Stamps were then cut out and sonicated in ethanol before each use. Stamps were dried under a nitrogen stream and then coated with a 50 μg/ml solution of fibronectin for 30 minutes. To check patterning, stamps were occasionally coated with a mixture of 50 μg/ml fibronectin, rabbit polyclonal anti-fibronectin antibody (Calbiochem, Gibbstown, NJ) at 1:10 dilution, and Alexa Fluor 488 goat anti-rabbit secondary antibody at 1:100 dilution. Before stamping, 35-mm glass bottom dishes were cleaned with ethanol and oxygen plasma. Dishes were stamped with fibronectin for 1 minute, heated to 140℃ for 30 seconds (Fink et al., 2007), and passivated with 0.1 mg/ml PLL(20)-g-[3,5]-PEG(2) (Susos AG, Dubendorf, Switzerland) in 10 mM HEPES (pH 7.4) for 30 minutes to render the unstamped regions of the dish resistant to cell adhesion (Thery and Piel, 2009). Plates were then washed in PBS and stored at 4℃ for up to 2 weeks or immediately used for cell seeding. Stamps were cleaned with Scotch tape (3M, St Paul, MN) after use.

Calculating MTOC and nucleus position

The position of the MTOC and nucleus are reported relative to each individual centroid of the cell, divided by its effective radius. Absolute MTOC and nucleus centroids were determined from γ-tubulin and DAPI immunofluorescence images, respectively, using Metamorph software. MTOCs were identified as either single or double spots of intensity near the nucleus; cells with multiple foci of intensity that were not adjacent to one another were omitted to avoid comparing interphase cells with mitotic cells. Cells were hand-traced and their areas and centroids were determined using the integrated morphometry analysis feature in Metamorph. The effective cell radius, r_{eff}, was calculated from the cell area, A, using $r_{\text{eff}}=\sqrt{A/\pi}$. Although somewhat artificial for non-circular cells (such as sparse or triangular cells), this metric normalizes cells by their area and thus allows for better quantitative comparison between cells of different shapes.

In Fig. 1e,f, note that the bins are normalized by cell radius, and not by area, such that the area of outer bins are larger than inner bins. If bins were normalized by area, either the number of bins or the size of the bin can vary while the other variable is held fixed. In the case of a fixed number of bins, e.g. five bins, the most central bin will span a large radial distance, leaving small rings, equal in area, towards the perimeter of the circle; this would effectively exaggerate the 'center' of the circle. Alternatively, the central bin can be fixed to a reasonable size, and the number of bins can then increase until the perimeter of the circle is reached. In this case, the number of bins is so large that the data become noisy. In both cases of area normalization, relationships between conditions become less apparent and more difficult to grasp; for these reasons, bins were established according to the cell radius.

MTOC–nucleus distances were computed directly from traced MTOC and nuclear regions using a custom Matlab program. Distances were scored as 0 μm when the MTOC centroid was located within the nuclear region.

Assessing cell polarization

Cell polarization was assessed by overlaying γ-tubulin and DAPI images and scoring images based on the position of the MTOC relative to the nucleus (Lee et al., 2005; Tzima et al., 2003). The fraction of cells that were polarized was scored binarily, where a cell whose MTOC was located left of a line vertically bisecting the nucleus received a 1, and a cell whose MTOC was located to the right of this line received a 0 (Fig. 1i). Polarization was also assessed more quantitatively by computing an extent of polarization of the cell using:

$$\text{Extent of polarization} = \sin\theta \bullet |\bar{M}|$$

where θ refers to the angle formed by the vertical bisector of the nucleus and the vector $\bar{M}$ pointing from the nucleus centroid to the MTOC centroid. This quantity reflects both the distance between the MTOC and nucleus centroids as well as the location of the MTOC relative to the nucleus.

Single cell motility assay

Each well of a 12-well glass bottom plate (MatTek) was coated with 500 μl of 50 μg/ml fibronectin for 1 hour for experimental consistency. After 72 hour siRNA transfection, MEFs were seeded into wells and incubated for 6 hours before imaging. MEFs were then tracked for 14 hours with a Nikon TE2000 controlled by NIS Elements (Nikon). Phase-contrast images were taken with a 10× Plan Fluor

Lens (NA 0.3; Nikon) every 2 minutes. Persistence time and length were quantified with Metamorph.

Stable cell line generation and live-cell imaging

MEFs were transfected with CETN2–RFP (courtesy of Joseph Gleeson, University of California, San Diego, CA), which was used to visualize centrin2, or the MTOC in live cells (Tanaka et al., 2004). Studies have confirmed microtubule regrowth from CETN2–RFP puncta after nocodazole washout, confirming that these puncta are capable of microtubule nucleation, corroborating evidence that centrin2 is an accurate centrosomal marker (Levy and Holzbaur, 2008). Forward transfection was carried out using Lipofectamine LTX (Invitrogen) according to the manufacturer's protocol. Stably transfected cells were selected using 1 mg/ml G418 (Mediatech, Manassas, VA). Colonies expressing adequate amounts of CETN2–RFP allowing for easy MTOC visualization were then selected and propagated.

For live-cell imaging, stably transfected MEFs were seeded on fibronectin-coated glass bottom dishes. Next, to visualize the nucleus, cells were incubated in 0.5 μM DRAQ5 (Cell Signaling) for 5 minutes at RT and subsequently washed in PBS before imaging. Time-lapse images were then collected using a Nikon A1 confocal galvano scanner mounted on a Nikon Eclipse Ti microscope (Nikon) with a 60× Plan Apo VC lens (NA 1.4; Nikon). During imaging, cells were maintained at 37℃ and 5% CO_2 using a stagetop incubator (Okolab, Naples, Italy). Images were acquired every 5 minutes for a total of 5 hours and subsequently analyzed using Elements software (Nikon).

Statistical analysis

Data are expressed as means ± s.e.m. and, unless indicated, were analyzed for significance by one-way ANOVA followed by Dunnett's multiple comparison test with Prism software (Graphpad, La Jolla, CA). For polarization values, populations were compared with an unpolarized population-based theoretical mean of 0.5 for the fraction of the cells that were polarized and 0.0 for the extent of horizontal polarization using one sample *t*-tests. Significant differences are indicated as follows: *** for $P<0.001$, ** for $P<0.01$ and * for $P<0.05$.

Acknowledgements

We thank Matthieu Piel for helping us with micropatterning.

Funding

This research was supported in part by the National Institutes of Health [grant numbers U54CA143868, R01 GM084204]. Deposited in PMC for release after 12 months.

Supplementary material available online at
http://jcs.biologists.org/lookup/suppl/doi:10.1242/jcs.091231/-/DC1

References

Bacallao, R., Antony, C., Dotti, C., Karsenti, E., Stelzer, E. H. and Simons, K. (1989). The subcellular organization of Madin-Darby canine kidney cells during the formation of a polarized epithelium. *J. Cell Biol.* **109**, 2817-2832.

Bajpai, S., Correia, J., Feng, Y., Figueiredo, J., Sun, S. X., Longmore, G. D., Suriano, G. and Wirtz, D. (2008). {alpha}-Catenin mediates initial E-cadherin-dependent cell-cell recognition and subsequent bond strengthening. *Proc. Natl. Acad. Sci. USA* **105**, 18331-18336.

Bergmann, J. E., Kupfer, A. and Singer, S. J. (1983). Membrane insertion at the leading edge of motile fibroblasts. *Proc. Natl. Acad. Sci. USA* **80**, 1367-1371.

Berzat, A. and Hall, A. (2010). Cellular responses to extracellular guidance cues. *EMBO J.* **29**, 2734-2745.

Bornens, M. (2008). Organelle positioning and cell polarity. *Nat. Rev. Mol. Cell Biol.* **9**, 874-886.

Burakov, A., Nadezhdina, E., Slepchenko, B. and Rodionov, V. (2003). Centrosome positioning in interphase cells. *J. Cell Biol.* **162**, 963-969.

Crisp, M., Liu, Q., Roux, K., Rattner, J. B., Shanahan, C., Burke, B., Stahl, P. D. and Hodzic, D. (2006). Coupling of the nucleus and cytoplasm: role of the LINC complex. *J. Cell Biol.* **172**, 41-53.

Doxsey, S. (2001). Re-evaluating centrosome function. *Nat. Rev. Mol. Cell Biol.* **2**, 688-698.

Dupin, I., Camand, E. and Etienne-Manneville, S. (2009). Classical cadherins control nucleus and centrosome position and cell polarity. *J. Cell Biol.* **185**, 779-786.

Etienne-Manneville, S. and Hall, A. (2001). Integrin-mediated activation of Cdc42 controls cell polarity in migrating astrocytes through PKCzeta. *Cell* **106**, 489-498.

Etienne-Manneville, S. and Hall, A. (2003). Cdc42 regulates GSK-3beta and adenomatous polyposis coli to control cell polarity. *Nature* **421**, 753-756.

Euteneuer, U. and Schliwa, M. (1992). Mechanism of centrosome positioning during the wound response in BSC-1 cells. *J. Cell Biol.* **116**, 1157-1166.

Fink, J., Thery, M., Azioune, A., Dupont, R., Chatelain, F., Bornens, M. and Piel, M. (2007). Comparative study and improvement of current cell micro-patterning techniques. *Lab. Chip.* **7**, 672-680.

Friedl, P. (2004). Prespecification and plasticity: shifting mechanisms of cell migration. *Curr. Opin. Cell Biol.* **16**, 14-23.

Giampieri, S., Manning, C., Hooper, S., Jones, L., Hill, C. S. and Sahai, E. (2009). Localized and reversible TGFbeta signalling switches breast cancer cells from cohesive to single cell motility. *Nat. Cell Biol.* **11**, 1287-1296.

Goley, E. D. and Welch, M. D. (2006). The ARP2/3 complex: an actin nucleator comes of age. *Nat. Rev. Mol. Cell Biol.* **7**, 713-726.

Gomes, E. R., Jani, S. and Gundersen, G. G. (2005). Nuclear movement regulated by Cdc42, MRCK, myosin, and actin flow establishes MTOC polarization in migrating cells. *Cell* **121**, 451-463.

Gotlieb, A. I., May, L. M., Subrahmanyan, L. and Kalnins, V. I. (1981). Distribution of microtubule organizing centers in migrating sheets of endothelial cells. *J. Cell Biol.* **91**, 589-594.

Gundersen, G. G. and Bulinski, J. C. (1988). Selective stabilization of microtubules oriented toward the direction of cell migration. *Proc. Natl. Acad. Sci. USA* **85**, 5946-5950.

Hale, C. M., Shrestha, A. L., Khatau, S. B., Stewart-Hutchinson, P. J., Hernandez, L., Stewart, C. L., Hodzic, D. and Wirtz, D. (2008). Dysfunctional connections between the nucleus and the actin and microtubule networks in laminopathic models. *Biophys. J.* **95**, 5462-5475.

Hale, C. M., Sun, S. X. and Wirtz, D. (2009). Resolving the role of actoymyosin contractility in cell microrheology. *PLoS ONE* **4**, e7054.

Higginbotham, H. R. and Gleeson, J. G. (2007). The centrosome in neuronal development. *Trends Neurosci.* **30**, 276-283.

Holgerson, P., Sutherland, D. S., Kasemo, B. and Chakarov, D. (2005). Patterning and modification of PDMS surface through laster micromachining of silicon masters and molding. *Appl. Phys. A* **81**, 51-56.

Jiang, X., Bruzewicz, D. A., Wong, A. P., Piel, M. and Whitesides, G. M. (2005). Directing cell migration with asymmetric micropatterns. *Proc. Natl. Acad. Sci. USA* **102**, 975-978.

Khatau, S. B., Hale, C. M., Stewart-Hutchinson, P. J., Patel, M. S., Stewart, C. L., Searson, P. C., Hodzic, D. and Wirtz, D. (2009). A perinuclear actin cap regulates nuclear shape. *Proc. Natl. Acad. Sci. USA* **106**, 19017-19022.

Khatau, S. B., Kim, D. H., Hale, C. M., Bloom, R. J. and Wirtz, D. (2010). The perinuclear actin cap in health and disease. *Nucleus* **1**, 337-342.

Kupfer, A., Louvard, D. and Singer, S. J. (1982). Polarization of the Golgi apparatus and the microtubule-organizing center in cultured fibroblasts at the edge of an experimental wound. *Proc. Natl. Acad. Sci. USA* **79**, 2603-2607.

Lee, J. S. H., Chang, M. I., Tseng, Y. and Wirtz, D. (2005). Cdc42 mediates nucleus movement and MTOC polarization in Swiss 3T3 fibroblasts under mechanical shear stress. *Mol. Biol. Cell* **16**, 871-880.

Lee, J. S. H., Hale, C. M., Panorchan, P., Khatau, S. B., George, J. P., Tseng, Y., Stewart, C. L., Hodzic, D. and Wirtz, D. (2007). Nuclear lamin A/C deficiency induces defects in cell mechanics, polarization, and migration. *Biophys. J.* **93**, 2542-2552.

Levy, J. R. and Holzbaur, E. L. (2008). Dynein drives nuclear rotation during forward progression of motile fibroblasts. *J. Cell Sci.* **121**, 3187-3195.

Li, R. and Gundersen, G. G. (2008). Beyond polymer polarity: how the cytoskeleton builds a polarized cell. *Nat. Rev. Mol. Cell Biol.* **9**, 860-873.

Lin, D., Edwards, A. S., Fawcett, J. P., Mbamalu, G., Scott, J. D. and Pawson, T. (2000). A mammalian PAR-3-PAR-6 complex implicated in Cdc42/Rac1 and aPKC signalling and cell polarity. *Nat. Cell Biol.* **2**, 540-547.

Malone, C. J., Misner, L., Le Bot, N., Tsai, M. C., Campbell, J. M., Ahringer, J. and White, J. G. (2003). The C-elegans hook protein, ZYG-12, mediates the essential attachment between the centrosome and nucleus. *Cell* **115**, 825-836.

Manneville, J. B. and Etienne-Manneville, S. (2006). Positioning centrosomes and spindle poles: looking at the periphery to find the centre. *Biol. Cell* **98**, 557-565.

Minc, N., Burgess, D. and Chang, F. (2011). Influence of cell geometry on division-plane positioning. *Cell* **144**, 414-426.

Nemere, I., Kupfer, A. and Singer, S. J. (1985). Reorientation of the Golgi apparatus and the microtubule-organizing center inside macrophages subjected to a chemotactic gradient. *Cell Motil.* **5**, 17-29.

Nobes, C. D. and Hall, A. (1999). Rho GTPases control polarity, protrusion, and adhesion during cell movement. *J. Cell Biol.* **144**, 1235-1244.

Palazzo, A. F., Joseph, H. L., Chen, Y. J., Dujardin, D. L., Alberts, A. S., Pfister, K. K., Vallee, R. B. and Gundersen, G. G. (2001). Cdc42, dynein, and dynactin regulate MTOC reorientation independent of Rho-regulated microtubule stabilization. *Curr. Biol.* **11**, 1536-1541.

Ponti, A., Machacek, M., Gupton, S. L., Waterman-Storer, C. M. and Danuser, G. (2004). Two distinct actin networks drive the protrusion of migrating cells. *Science* **305**, 1782-1786.

Razafsky, D. and Hodzic, D. (2009). Bringing KASH under the SUN: the many faces of nucleo-cytoskeletal connections. *J. Cell Biol.* **186**, 461-472.

Reinsch, S. and Gonczy, P. (1998). Mechanisms of nuclear positioning. *J. Cell Sci.* **111**, 2283-2295.

Salpingidou, G., Smertenko, A., Hausmanowa-Petrucewicz, I., Hussey, P. J. and Hutchison, C. J. (2007). A novel role for the nuclear membrane protein emerin in association of the centrosome to the outer nuclear membrane. *J. Cell Biol.* **178**, 897-904.

Schiff, P. B., Fant, J. and Horwitz, S. B. (1979). Promotion of microtubule assembly in vitro by taxol. *Nature* **277**, 665-667.

Schmoranzer, J., Fawcett, J. P., Segura, M., Tan, S., Vallee, R. B., Pawson, T. and Gundersen, G. G. (2009). Par3 and dynein associate to regulate local microtubule dynamics and centrosome orientation during migration. *Curr. Biol.* **19**, 1065-1074.

Singer, A. J. and Clark, R. A. (1999). Cutaneous wound healing. *N. Engl. J. Med.* **341**, 738-746.

Stewart-Hutchinson, P. J., Hale, C. M., Wirtz, D. and Hodzic, D. (2008). Structural requirements for the assembly of LINC complexes and their function in cellular mechanical stiffness. *Exp. Cell Res.* **314**, 1892-1905.

Sullivan, T., Escalante-Alcalde, D., Bhatt, H., Anver, M., Bhat, N., Nagashima, K., Stewart, C. L. and Burke, B. (1999). Loss of A-type lamin expression compromises nuclear envelope integrity leading to muscular dystrophy. *J. Cell Biol.* **147**, 913-919.

Svitkina, T. M., Verkhovsky, A. B. and Borisy, G. G. (1996). Plectin sidearms mediate interaction of intermediate filaments with microtubules and other components of the cytoskeleton. *J. Cell Biol.* **135**, 991-1007.

Tanaka, T., Serneo, F. F., Higgins, C., Gambello, M. J., Wynshaw-Boris, A. and Gleeson, J. G. (2004). Lis1 and doublecortin function with dynein to mediate coupling of the nucleus to the centrosome in neuronal migration. *J. Cell Biol.* **165**, 709-721.

Thery, M. (2010). Micropatterning as a tool to decipher cell morphogenesis and functions. *J. Cell Sci.* **123**, 4201-4213.

Thery, M. and Piel, M. (2009). Adhesive micropatterns for cells: a microcontact printing protocol. *Cold Spring Harb. Protoc.* **2009**, pdb prot5255.

Thery, M., Racine, V., Piel, M., Pepin, A., Dimitrov, A., Chen, Y., Sibarita, J. B. and Bornens, M. (2006). Anisotropy of cell adhesive microenvironment governs cell internal organization and orientation of polarity. *Proc. Natl. Acad. Sci. USA* **103**, 19771-19776.

Thiery, J. P., Acloque, H., Huang, R. Y. and Nieto, M. A. (2009). Epithelial-mesenchymal transitions in development and disease. *Cell* **139**, 871-890.

Todaro, G. J., Lazar, G. K. and Green, H. (1965). The initiation of cell division in a contact-inhibited mammalian cell line. *J. Cell Physiol.* **66**, 325-333.

Trinkaus, J. P. (1984). *Cells into Organs: The Forces That Shape the Embryo*. Englewood CliffsNJ: Prentice Hall.

Tsai, J. W., Bremner, K. H. and Vallee, R. B. (2007). Dual subcellular roles for LIS1 and dynein in radial neuronal migration in live brain tissue. *Nat. Neurosci.* **10**, 970-979.

Tynan, S. H., Purohit, A., Doxsey, S. J. and Vallee, R. B. (2000). Light intermediate chain 1 defines a functional subfraction of cytoplasmic dynein which binds to pericentrin. *J. Biol. Chem.* **275**, 32763-32768.

Tzima, E., Kiosses, W. B., del Pozo, M. A. and Schwartz, M. A. (2003). Localized Cdc42 activation, detected using a novel assay, mediates microtubule organizing center positioning in endothelial cells in response to fluid shear stress. *J. Biol. Chem.* **278**, 31020-31023.

Waterman-Storer, C. M. and Salmon, E. D. (1997). Actomyosin-based retrograde flow of microtubules in the lamella of migrating epithelial cells influences microtubule dynamic instability and turnover and is associated with microtubule breakage and treadmilling. *J. Cell Biol.* **139**, 417-434.

Weis, W. I. and Nelson, W. J. (2006). Re-solving the cadherin-catenin-actin conundrum. *J. Biol. Chem.* **281**, 35593-35597.

Wilhelmsen, K., Litjens, S. H. M., Kuikman, I., Tshimbalanga, N., Janssen, H., van den Bout, I., Raymond, K. and Sonnenberg, A. (2005). Nesprin-3, a novel outer nuclear membrane protein, associates with the cytoskeletal linker protein plectin. *J. Cell Biol.* **171**, 799-810.

Wolf, K., Mazo, I., Leung, H., Engelke, K., von Andrian, U. H., Deryugina, E. I., Strongin, A. Y., Brocker, E. B. and Friedl, P. (2003). Compensation mechanism in tumor cell migration: mesenchymal-amoeboid transition after blocking of pericellular proteolysis. *J. Cell Biol.* **160**, 267-277.

Worman, H. J. and Gundersen, G. G. (2006). Here come the SUNs: a nucleocytoskeletal missing link. *Trends Cell Biol.* **16**, 67-69.

Zhao, M., Song, B., Pu, J., Wada, T., Reid, B., Tai, G., Wang, F., Guo, A., Walczysko, P., Gu, Y. et al. (2006). Electrical signals control wound healing through phosphatidylinositol-3-OH kinase-gamma and PTEN. *Nature* **442**, 457-460.

Zhen, Y. Y., Libotte, T., Munck, M., Noegel, A. A. and Korenbaum, E. (2002). NUANCE, a giant protein connecting the nucleus and actin cytoskeleton. *J. Cell Sci.* **115**, 3207-3222.

Zhu, J., Burakov, A., Rodionov, V. and Mogilner, A. (2010). Finding the cell center by a balance of dynein and myosin pulling and microtubule pushing: a computational study. *Mol. Biol. Cell* **21**, 4418-4427.